

PAPER • OPEN ACCESS

Crack deflection in laminates with graded stiffness—lessons from biology

To cite this article: Israel Greenfeld and H Daniel Wagner 2023 *Bioinspir. Biomim.* **18** 036001

View the [article online](#) for updates and enhancements.

You may also like

- [Structural analysis across length scales of the scorpion pincer cuticle](#)
Israel Kellersztein, Israel Greenfeld and H Daniel Wagner
- [Morphology, nano-mechanical properties and bending fracture stress of hind leg material of *Cybister japonicus* beetle](#)
Zhixian Yang, Ming Zhang and Chao Zhang
- [Model for simulating scorpion substrate vibration and detection system](#)
B A Sadiq, A M Aibinu, E Joseph et al.

Bioinspiration & Biomimetics



PAPER

Crack deflection in laminates with graded stiffness—lessons from biology

OPEN ACCESS

RECEIVED
5 December 2022

REVISED
3 February 2023

ACCEPTED FOR PUBLICATION
2 March 2023

PUBLISHED
17 March 2023

Israel Greenfeld*  and H Daniel Wagner* 

Department of Molecular Chemistry and Materials Science, Weizmann Institute of Science, Rehovot 76100, Israel

* Authors to whom any correspondence should be addressed.

E-mail: green_is@netvision.net.il and Daniel.Wagner@weizmann.ac.il

Keywords: laminate, crack, propagation, delamination, deflection, scorpion, cuticle

Original content from this work may be used under the terms of the [Creative Commons Attribution 4.0 licence](https://creativecommons.org/licenses/by/4.0/).

Any further distribution of this work must maintain attribution to the author(s) and the title of the work, journal citation and DOI.



Abstract

A crack propagating through a laminate can cause severe structural failure, which may be avoided by deflecting or arresting the crack before it deepens. Inspired by the biology of the scorpion exoskeleton, this study shows how crack deflection can be achieved by gradually varying the stiffness and thickness of the laminate layers. A new generalized multi-layer, multi-material analytical model is proposed, using linear elastic fracture mechanics. The condition for deflection is modeled by comparing the applied stress causing a cohesive failure, resulting in crack propagation, to that causing an adhesive failure, resulting in delamination between layers. We show that a crack propagating in a direction of progressively decreasing elastic moduli is likely to deflect sooner than when the moduli are uniform or increasing. The model is applied to the scorpion cuticle, the laminated structure of which is composed of layers of helical units (Bouligands) with inward decreasing moduli and thickness, interleaved with stiff unidirectional fibrous layers (interlayers). The decreasing moduli act to deflect cracks, whereas the stiff interlayers serve as crack arrestors, making the cuticle less vulnerable to external defects induced by its exposure to harsh living conditions. These concepts may be applied in the design of synthetic laminated structures to improve their damage tolerance and resilience.

1. Introduction

A major challenge in engineering design is to ensure structural integrity of a product throughout its intended life cycle. Designers typically apply standard safety margins to account for the uncertainty and variability in loads, material properties, and environmental conditions. Such conventional design approach is not optimal as it results in overdesign and excessive costs. Structures designed for damage tolerance are more efficient and resilient, as they can sustain inherent material flaws and their growth during service. Propagating cracks can be detrimental and even catastrophic, and therefore design measures are taken to contain them by arresting, bridging, or diversion. For example, a crack starting at the surface of a structure and propagating deeply into it, can be forced to deflect perpendicularly in order to avoid catastrophic failure. In composite laminates, a deflected surface crack causes delamination between

laminae, absorbing energy by deforming and tearing the interlaminar adhesive [1].

Nature excels in optimizing structures for resilience and self-healing, given the limited available resources and the high costs involved in building structural tissues. Our recent communication reviews the various architectural strategies used in nature, most notably layered composite structures and complex geometries, and introduces the notion of hierarchical interfaces [1]. Elaborate micro-structural mechanisms are implemented in biology to combine strength and toughness, often conflicting properties, and may inspire engineering design [2]. One such measure involves orientation and anisotropy, which are designed into biological structures to achieve diverse functionalities [3]. Another measure is the introduction of soft interfaces into ceramics and ceramic-based composites to overcome their inherent brittleness by deflecting cracks [4–6]. Interfaces have a key role in controlling the deformation

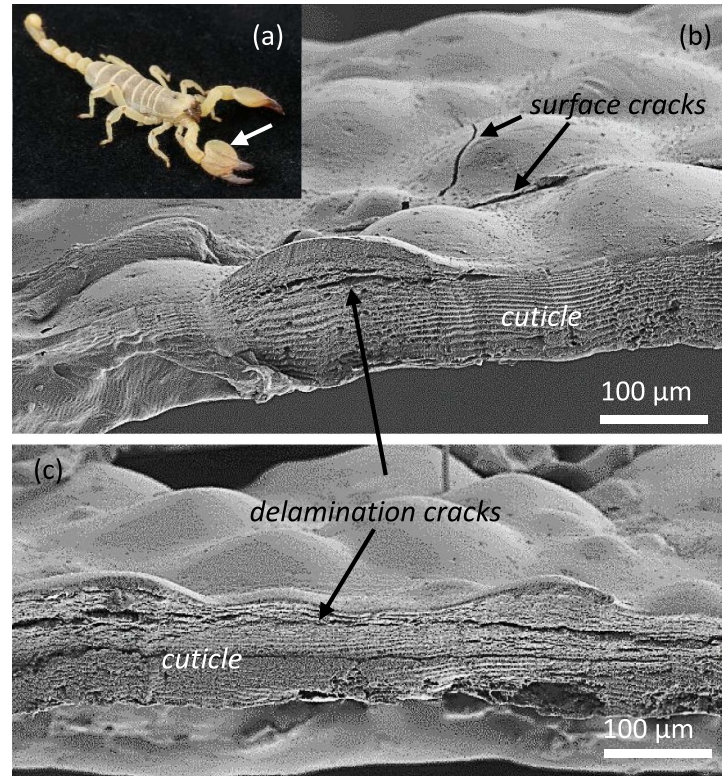


Figure 1. Cracks in the scorpion exoskeleton after loading. (a) *Scorpio Maurus Palmatus*, the chela (pincer) is marked by arrow. (b) Cross section through the chela cuticle after bending test, showing surface propagating (Griffith) cracks and delamination cracks. (c) Long delamination crack close to the cuticle surface (Adapted from [16]). © IOP Publishing Ltd. All rights reserved).

and toughness of composites constructed from hard building blocks, such as the ceramic platelets in bone, by channeling the propagation of cracks [7–9]. Yet another approach is the variable thickness of layers in a laminated structure, found in the gradually decreasing silica layers in the sponge spicule, which is shown to impact the structural strength [10–12]. Thin layers are found to limit the penetration depth of cracks by forcing early deflection, thus enhancing toughness and survivability [13], and, furthermore, below a certain critical size, materials are shown to become insensitive to flaws at nanoscale [14].

A representative biological example of a complex laminated structure, which is in the focus of the current study, is the scorpion exoskeletal cuticle [15, 16]. The cuticle is arranged in eight hierarchical levels and respective interfaces: (from bottom to top) α -chitin molecules, chitin-protein fibrils and fibers, unidirectional fibrous laminae, helical laminate assemblies (Bouligands), and stacks of Bouligands and unidirectional layers. See detailed illustrations in [17] (figure 6) and in [15] (figure 1). This structure is strong and tough, with the ability to deflect Griffith cracks propagating from the surface, to perpendicular delamination cracks propagating between layers (figures 1(a) and (b)). Delamination cracks can be very long (figure 1(c)), thus dissipating a large amount of energy, but more importantly, they occur

fairly close to the cuticle surface, thereby blocking the propagation of surface cracks at an early stage and maintaining structural integrity with only partial functional degradation.

Whether a crack tends to propagate parallel to itself in a Griffith-like fashion or to bifurcate in a deflected direction (not necessarily perpendicular to its original path) has been extensively studied for the bilayer case but not for the general case of graded, multilayer (with variable thickness), multi-material structures. Early analytical and numerical models were restricted to crack propagation and/or bifurcation between elastic bi-material layers only [18–26]. Rare models have been proposed for laminates with a large number of alternating bi-material layers of equal thickness [27]. However, very few, if any, models exist for functionally graded bi- or multi-material laminates, which are necessary for addressing the high complexity of natural structures. Such models may answer the key question whether graded properties (stiffness and thickness) confer advantages to natural structures, which could be used as inspiration in engineering laminates. Hence, the purpose of the current study is to develop a new generalized analytical model for crack deflection in a multi-layer, multi-material laminate, and apply it to a biological laminate such as the scorpion's cuticle.

Here, we start by calculating the applied stresses which may cause a propagation or delamination failure in a discretely anisotropic inhomogeneous laminate under in-plane uniaxial tension. The approach is based on ideas developed by Kendall in the 1970s for a dual-layer structure [18], with generalization to a multi-layer laminate, which has varying laminae thicknesses and mechanical properties. We proceed with defining the criterion for deflecting a crack from propagation to delamination, and apply it to a general case of a laminate with graded moduli. The application to a biological tissue is then described, with focus on the scorpion cuticle, including the effect of varying laminae thickness and stiffness, as well as stiffness discontinuity between adjacent laminae. We demonstrate how the gradation of laminae stiffness can enhance structural integrity without sacrificing strength.

2. Theory of crack deflection in laminates

A general laminated structure is highly complex, as it exhibits anisotropy of stiffness, strength and fracture toughness in all three directions, as well as inhomogeneity of these properties across layers. A crack in a layered laminate can advance either by propagation across laminae (a Griffith crack), or by delamination of the interface between laminae. When propagating towards an interface, it may advance either way, depending on the local and global elastic properties, the local fracture energies for propagation (cohesive energy) and delamination (adhesive energy), the crack depth, the geometry of the laminate, and the type of load applied on it. From toughness and structural reliability points of view, crack advancement by delamination is preferred over propagation, as it dissipates energy during failure while gracefully degrading the structural integrity, whereas propagation can result in fast catastrophic failure.

2.1. Anisotropic inhomogeneous laminate

Consider a layered laminate of thickness d and width w , infinite in the x direction, made of successive laminae numbered $i = [1..n]$, whose thickness is t_i (figure 2). The mechanical properties of lamina i in the x direction are its stiffness E_i , cohesive fracture energy $G_{co,i}$, and adhesive fracture energy $G_{ad,i}$. These properties are uniform throughout the lamina's own thickness, but vary across the laminate thickness, so that the laminate is inhomogeneous in the z direction. The laminate is subjected to a uniform in-plane stress σ in the x direction. A Griffith crack of length c , perpendicular to the loading direction, propagates towards an interface located within lamina k , and can either proceed in a self-similar fashion or deflect perpendicularly along a length l within the interface. The

laminae mechanical properties are anisotropic within the xy plane, and therefore vary with respect to a given loading direction.

2.2. Cohesive and adhesive failure stresses

According to fracture mechanics, a Griffith crack in a plate under load will propagate when its growth releases an amount of stored elastic energy large enough to break the chemical bonds across the crack. In formal terms, the condition for crack instability, that is propagation, is obtained by equating the rate of change of the elastic energy released in the region above the crack tip by a growing cohesive crack, to the rate of change of the surface energy gained by the crack. The work done by the applied stress is ignored, as the displacement of the region below the crack tip is negligible. This leads to the following expression for the stress causing further propagation of the crack (breaking of bonds across a layer, or cohesive failure)—see details in the [appendix](#):

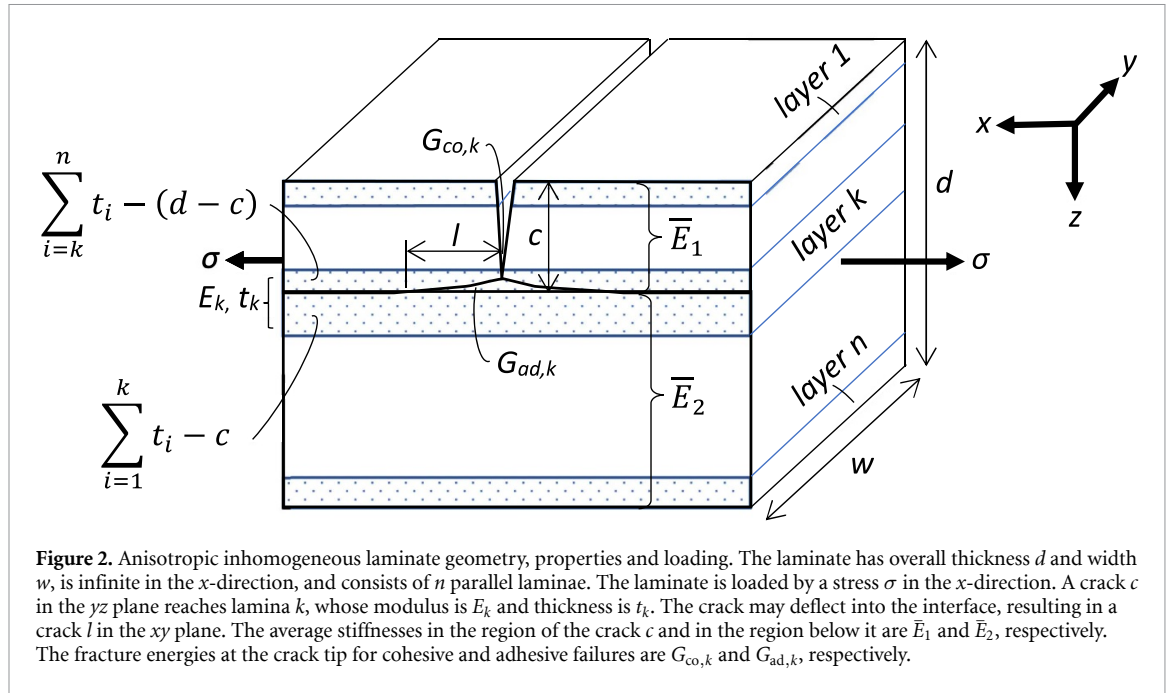
$$\sigma_{co} = \bar{E} \left[\frac{G_{co}}{\pi c \bar{E}_1 (1 - \nu^2)} \right]^{1/2} = \sqrt{\frac{G_{co} \bar{E}}{\pi c (1 - \nu^2)}} \sqrt{\frac{\bar{E}}{\bar{E}_1}} \quad (1)$$

where \bar{E} is the weighted-average in-plane stiffness of the entire laminate, \bar{E}_1 is the weighted-average stiffness in the laminate upper region, G_{co} is the cohesive fracture energy at the crack tip, and the term $1 - \nu^2$ is the effect of Poisson's ratio in plane strain condition (e.g. in thick laminates), removed in plane stress condition. A weighted-average is obtained by summing up the stiffnesses of the individual layers, each weighted by its own thickness. Equation (1) has two terms: the classic Griffith relation (first square-root), where $\sqrt{G_{co} \bar{E} / (1 - \nu^2)} \equiv K_c$ is defined as the laminate fracture toughness, and an inhomogeneity correction factor (second square-root). For a homogeneous plate (uniform stiffness, $\bar{E}_1 = \bar{E} = E$), the correction factor is 1 and the classic Griffith relation is recovered. Substituting the average stiffnesses \bar{E} and \bar{E}_1 (see equation (32) in the [appendix](#)), the stress causing propagation (cohesive failure) is obtained in a discrete form containing the explicit mechanical properties of each layer:

$$\sigma_{co} = \frac{1}{d} \left[\frac{G_{co,k}}{\pi (1 - \nu^2)} \right]^{1/2} \left(\sum_{i=1}^n E_i t_i \right) \times \left[\frac{1}{\sum_{i=1}^k E_i t_i - E_k \left(\sum_{i=1}^k t_i - c \right)} \right]^{1/2} \quad (2)$$

where $G_{co,k}$ is the cohesive fracture energy at lamina k .

Similarly, a delamination crack in a plate under load will advance when its growth releases a net amount of stored elastic energy large enough to break the chemical bonds across the interface. In formal terms, the condition for crack instability in



delamination is obtained by equating the net change rate of the elastic energy released in the region above the crack tip and the elastic energy gained in the region below the crack tip by a growing adhesive crack, to the change rate of the surface energy gained by the crack. Additional energy is invested in the crack by the work done by the applied stress as a result of the elastic displacement of the region below the crack tip. This leads to the following expression for the stress causing delamination (debonding of an interface between layers, or adhesive failure)—see details in the [appendix](#):

$$\sigma_{ad} = \left[\frac{2G_{ad}\bar{E}}{c} \left(1 - \frac{c}{d}\right) \frac{\bar{E}_2}{\bar{E}_1} \right]^{1/2} = \sqrt{\frac{2G_{ad}\bar{E}}{c} \left(1 - \frac{c}{d}\right)} \sqrt{\frac{\bar{E}_2}{\bar{E}_1}} \quad (3)$$

where \bar{E}_2 is the weighted-average stiffness in the laminate lower region, and G_{ad} is the adhesive fracture energy at the crack tip. Note that the stress causing adhesive failure is independent of the crack length l . Equation (3) has two terms: a Griffith-like relation in which G_{co} is replaced by G_{ad} (first square-root), and an inhomogeneity correction factor (second square-root) which tends to 1 for homogenous plate ($\bar{E}_1 = \bar{E}_2$). Substituting the average stiffnesses \bar{E} , \bar{E}_1 and \bar{E}_2 (see equation (32) in the [appendix](#)), the stress causing delamination (adhesive failure) is obtained in a discrete form containing the explicit mechanical properties of each layer:

$$\sigma_{ad} = \frac{1}{d} \left[2G_{ad,k} \left(\sum_{i=1}^n E_i t_i \right) \times \frac{\sum_{i=k}^n E_i t_i - E_k \left(\sum_{i=k}^n t_i - d + c \right)}{\sum_{i=1}^k E_i t_i - E_k \left(\sum_{i=1}^k t_i - c \right)} \right]^{1/2} \quad (4)$$

where $G_{ad,k}$ is the adhesive fracture energy at lamina k . This equation is the same as Wagner’s equation for interfacial failure in a laminate (with minor adaptation of indices) [28, 29].

We see that the modeling by Kendall for cohesive and adhesive failures in a bi-material plate [18], can be adapted to a general multilayer laminate as well, by substituting weighted-average moduli for the regions above and below the crack tip (equations (1) and (3)). This applies also to the criterion for crack deflection from propagation to delamination described in the next section. Furthermore, we see that, although the fracture energies $G_{co}(z)$ and $G_{ad}(z)$ vary with the depth z in the laminate, the values that matter for the cohesive and adhesive stresses are those at the crack tip ($z = c$), $G_{co} = G_{co}(c)$ (equation (24)) and $G_{ad} = G_{ad}(c)$ (equation (28)).

Both insights, obtained formally from the mathematical formulation in the [appendix](#), are quite intuitive. The elastic energy released during crack advancement, whether by propagation or by delamination, is stored in the bulk regions above and below the crack tip. In addition, the elastic strain of these regions tends to be uniform across their layers because regions at different depth z are attached firmly together and therefore deflect about the same in the loading direction. Thus, when integrating the elastic energy along z we get an average modulus weighted by the local thickness dz . On the other hand, the fracture energies that are relevant to crack advancement are those of the material at the crack forefront (the leading tip), and are not affected by the history of the crack trajectory.

For small cracks, both the cohesive and adhesive stress expressions converge to the form

$$\sigma \propto \bar{E} \left[\frac{G}{c\bar{E}_1} \right]^{\frac{1}{2}} = \sqrt{\frac{G\bar{E}}{c}} \sqrt{\frac{\bar{E}}{\bar{E}_1}} \quad (5)$$

except for a different numerical prefactor. This relationship is obtained realizing that $\bar{E}_2 \cong \bar{E}$ for a small crack, and has two terms: the classic Griffith-like relation (first square-root), and an inhomogeneity correction factor (second square-root). Equation (5) tells us that the smaller \bar{E}_1 , the more difficult it is for a crack to advance. In other words, whether the failure is cohesive or adhesive, a higher stress will be required to advance a crack from a compliant media (\bar{E}_1) to a stiff media (\bar{E}_2), and vice versa.

2.3. Crack deflection from propagation to delamination

The deflection of a propagating crack to delamination is, as noted before, a preferred situation for toughness and reliability. Such deflection will occur when the stress causing an adhesive failure is lower than the stress causing a cohesive failure, that is,

$$\sigma_{ad} < \sigma_{co}. \quad (6)$$

Substituting the cohesive and adhesive stresses from equations (1) and (3) and rearranging, we obtain the criterion for crack deflection from cohesive failure to adhesive failure:

$$\frac{G_{ad}}{G_{co}} < \frac{1}{4\pi(1-\nu^2)(1-c/d)} \frac{\bar{E}}{\bar{E}_2} \quad (7)$$

where \bar{E} and \bar{E}_2 are the weighted-average in-plane moduli of the entire laminate and of the portion beyond the crack tip, respectively, and G_{ad} and G_{co} are the adhesive and cohesive fracture energies at the layer reached by the crack tip, respectively. A factor of $\sqrt{2}$ was added to the stress of an adhesive crack to account for crack initiation [18, 28, 30]. Substituting the average stiffnesses \bar{E} and \bar{E}_2 (see equation (32) in the appendix), the deflection criterion is obtained in a discrete form containing the explicit mechanical properties of each layer:

$$\frac{G_{ad,k}}{G_{co,k}} < \frac{1}{4\pi(1-\nu^2)} \frac{\sum_{i=1}^n E_i t_i}{\sum_{i=k}^n E_i t_i - E_k (\sum_{i=k}^n t_i - d + c)}. \quad (8)$$

The cohesive and adhesive failure stresses in equations (1) and (3) are a good approximation for short cracks, whereas for long cracks (when the ratio between crack length and laminate thickness, c/d , is high) a correction factor <1 should be incorporated to account for the increased stress intensity near the crack. See for example AFGROW Handbook [31]. That stress field affects the elastic energy stored in the structure and the corresponding strain energies released during crack advancement. As both crack types are exposed to the same stress field, the effect should be similar in both. Therefore we estimate, for

the purpose of the current analysis, that a similar factor applies for both stress types. As a result, this stress intensity factor would cancel in equation (6), and therefore the crack deflection analysis should apply for long cracks as well as for short cracks.

Equations (7) and (8) demonstrate that, as the crack c grows, the equation's right side increases, giving way to higher tendency for deflection. The reason for this becomes clear when observing the evolution of the strain release and gain regions in figure 10. In both failure types, the strain release regions are above the crack tip and therefore increase in proportion to the crack growth; however, in a delamination failure, there is in addition a strain gain region below the crack tip, which gradually diminishes with the crack growth, consequently increasing the net energy available for delamination as the propagation crack grows. Thus, the adhesive fracture stress decreases faster with c than the cohesive fracture stress, resulting in higher likelihood for deflection.

The higher \bar{E}_2 , the more difficult it is for a crack to deflect from propagation to delamination. In other words, when a propagating crack enters a stiffer media (\bar{E}_2), it will tend to continue propagating rather than deflecting perpendicularly. Conversely, a crack propagating from stiff (\bar{E}_1) to compliant (\bar{E}_2) media will find it easier to deflect. This trend looks, at first sight, counter-intuitive because it seems reasonable to assume that a propagating crack will be deterred from entering stiff media. However there is no contradiction here because, at the same time, deflecting perpendicularly becomes even more difficult, as can be seen from the ratio $\sigma_{ad}/\sigma_{co} \propto (\bar{E}_2/\bar{E})^{1/2}$ (obtained by dividing equation (3) by equation (1)), which means that when entering stiffer media (\bar{E}_2 is higher), the stress required for adhesive failure is higher, resulting in higher tendency for continued self-similar crack propagation.

This argument refers to the expression at the right side of the inequality in equation (7), which accounts for the elastic stiffnesses and their variation with respect to the laminate structure and the crack length. However, the energies ratio in the left side of the inequality, G_{ad}/G_{co} , varies with respect to the same variables as well. For instance, in a laminated fiber composite, the in-plane modulus depends on the fibers volume fraction, such that a higher fraction of fibers will yield higher \bar{E}_2 . Similarly, the cohesive energy released by crack advancement, G_{co} , which is dominated by the strong fibrous elements in the structure, will be higher for higher fibers fraction. Consequently, both sides of equation (7) will change in proportion to the fiber fraction, \bar{E}_2 with respect to the fraction in the layers beyond the crack tip, and G_{co} with respect to the local fraction at the crack tip. The combined effect on the deflection criterion in brittle materials is analyzed in detail and presented in section 2.4, and demonstrated for two cases (the

graded moduli case, and the scorpion's endocuticle case) in sections 2.5 and 3.2.

For small cracks, both criteria (7) and (8) converge to the form [18]

$$\frac{G_{ad}}{G_{co}} < \frac{1}{4\pi(1-\nu^2)} \tag{9}$$

This relationship is obtained when realizing that $\bar{E}_2 \cong \bar{E}$ for a small crack. This means that for small cracks the elastic moduli do not play a role in the deflection process, regardless of the material inhomogeneity.

In layered composites, a crack often adopts a step-wise trajectory, where it starts propagating perpendicularly to the laminate, then deflects horizontally by delamination along an interface, then returns to propagation and keeps alternating between delamination and propagation until complete failure. As discussed previously, delamination failure is preferred for toughness and reliability, because it dissipates energy without causing a catastrophic failure, and therefore reverting a crack back to propagation might be an undesired occurrence. Apparently, reverting a crack from delamination to propagation requires moving the crack initiation factor of $\sqrt{2}$, applied to the adhesive failure stress, to the cohesive failure stress, resulting in overcoming a stress threshold factor of $\sqrt{2}\sqrt{2} = 2$. This stress threshold is equivalent to overcoming an energy threshold factor of $2^2 = 4$, as $G \propto \sigma^2$ (equation (5)). Thus, reversion is unlikely, unless the delamination ran its course, or a separate Griffith crack (due to a defect) was encountered that is deep enough to reach a new layer having a much lower G_{co} (by more than a factor of 4) and/or a much higher G_{ad} . Such abrupt fracture energy changes between layers are met, for example, in the alternating structure of unidirectional interlayers and quasi isotropic Bouligand layers in the scorpion's endocuticle (this is discussed in section 3.2) [15, 16]. The mean length l before crack deflection back to propagation would be $\sim 1/\bar{\lambda}_d$, where $\bar{\lambda}_d$ is the linear density of defects in the loading direction. Further analysis on this subject is not in the scope of the current study.

2.4. Failure stresses and crack deflection in brittle materials

The values of the cohesive and adhesive fracture energies G_{co} and G_{ad} in equations (1)–(4), (7) and (8) vary with respect to the specific location c of the crack tip in the laminate, and are not readily accessible for direct measurement or theoretical predictions in microscale and nanoscale laminates. However, for brittle materials, some assumptions and approximations may be made. In brittle materials, the fracture energy is proportional to the material tensile modulus, assuming no (or very little) plastic deformation around the crack tip [32]. This dependence can be expressed by equating the local ratio of cohesive energy/modulus to the global average ratio, $G_{co}/E \approx$

\bar{G}_{co}/\bar{E} , where \bar{G}_{co} is the average cohesive fracture energy of the entire laminate. Thus, we may approximate the cohesive fracture energy by

$$G_{co} \approx \frac{\bar{G}_{co}}{\bar{E}} E. \tag{10}$$

\bar{G}_{co} can be estimated from fracture toughness measurements of entire laminates. So, the variability of G_{co} , with respect to the location of the crack tip in the laminate, is replaced by that of E which is better known. The prefactor \bar{G}_{co}/\bar{E} is accessible experimentally and theoretically because these are average properties of the entire laminate. Similarly, the value of G_{ad} can be approximated by invoking again the proportionality between the fracture energy and the modulus in brittle materials, expressed by equating the local ratio of adhesive energy/modulus to the global average ratio, $G_{ad}/E_{ad} \approx \bar{G}_{co}/\bar{E}$, where E_{ad} is the stiffness of the interface between laminae. Thus, we may approximate the adhesive fracture energy by

$$G_{ad} \approx \frac{\bar{G}_{co}}{\bar{E}} E_{ad} \tag{11}$$

where the variability of G_{ad} is replaced by that of E_{ad} which is better known, with the same prefactor as in equation (10).

Substituting G_{co} from equation (10) in equation (1), we get the cohesive failure stress for a brittle structure:

$$\sigma_{co} = \left[\frac{\bar{G}_{co} \bar{E} E}{\pi c \bar{E}_1 (1-\nu^2)} \right]^{1/2} \tag{12}$$

which in the discrete form is (equation (2) rearranged)

$$\sigma_{co} = \left[\frac{\bar{G}_{co}}{\pi d (1-\nu^2)} \frac{E_k \sum_{i=1}^n E_i t_i}{\sum_{i=1}^k E_i t_i - E_k \left(\sum_{i=1}^k t_i - c \right)} \right]^{1/2} \tag{13}$$

Similarly, we may substitute G_{ad} from equation (11) in equations (3) and (4), in order to get the adhesive failure stress for a brittle structure. However, this is not necessary, as we may assume for simplicity that the adhesive failure energy is constant throughout the laminate, a property of the bonding matrix. Thus, the adhesive failure stress equations remain unchanged, but the constant value of G_{ad} or $G_{ad,k}$ can be estimated by equation (11).

The deflection condition for a brittle structure is obtained by substituting G_{co} from equation (10) in equation (7):

$$\frac{G_{ad}}{\bar{G}_{co}} < \frac{1}{4\pi(1-\nu^2)(1-c/d)} \frac{E}{\bar{E}_2}. \tag{14}$$

Note that the variable E on the right side is not an average but the local stiffness at the crack tip.

A corresponding inequality for a brittle structure is obtained for the discrete expression (equation (8)):

$$\frac{G_{ad,k}}{\bar{G}_{co}} < \frac{1}{4\pi(1-\nu^2)} \frac{E_k d}{\sum_{i=k}^n E_i t_i - E_k (\sum_{i=k}^n t_i - d + c)} \quad (15)$$

Here as well, the constant value of G_{ad} or $G_{ad,k}$ can be estimated by equation (11). Alternatively, when G_{ad} is not constant, one may substitute the relationship $G_{ad}/\bar{G}_{co} \approx E_{ad}/\bar{E}$ from equation (11) in equations (14) and (15), making the deflection condition independent of the fracture energies, dependent only on the elastic moduli. Specifically, the condition will depend on the local adhesive stiffness E_{ad} and the local layer stiffness E . Note that the source equations (equations (7) and (8)) apply to both ductile and brittle materials, such that G_{co} and G_{ad} each may include both elastic and plastic components, but, as said, these equations are not as useful due to the variability of G_{co} .

2.5. Crack deflection in a laminate with linearly graded moduli

This particular case, somewhat reminiscent of the graded moduli in the scorpion's cuticle (discussed in detail in section 3), demonstrates the impact of modulus gradation on crack deflection. The following gradation analysis makes use of the crack deflection theory just described. Consider a laminate with linearly graded modulus ranging from $\bar{E} - \Delta E$ to $\bar{E} + \Delta E$, expressed by

$$E = \bar{E} + \left(2\frac{z}{d} - 1\right) \Delta E \quad (16)$$

where \bar{E} is the weighted-average stiffness of the entire laminate, and ΔE is the moduli grading range (see example in the inset in figure 3). A positive (negative) ΔE indicates increasing (decreasing) moduli. The modulus at the crack tip is obtained by setting $z = c$. Using this relation in the failure stresses and deflection condition equations (see details in the appendix 'Linearly graded moduli'), we obtain their dependence on the crack length, depicted in the plots in figures 3 and 4, respectively.

These plots demonstrate that: (i) the failure stress decreases as the crack is longer, in all cases; (ii) the stress decreasing rate is steeper in the adhesive stress compared to the cohesive stress, in all cases, so that delamination takes over at a certain crack length where the adhesive stress becomes smaller than the cohesive stress; and (iii) deflection is more likely to occur when the crack is propagating towards layers with gradually decreasing moduli. In other words, crack deflection from propagation to delamination tends to occur earlier (at smaller c) when the layers moduli are decreasing in the direction of the crack growth. Conversely, when the layers moduli

are increasing, deflection would occur at a longer crack, even longer than for deflection in a homogenous laminate.

The cohesive and adhesive failure stresses in the example in figure 3 are calculated using the following typical bio-material data: (i) average modulus $\bar{E} = 8$ GPa, based on nanoindentation tests of the scorpion endocuticle ($\bar{E} = 7.3 - 8.5$ GPa) [17]; (ii) average cohesive fracture energy $\bar{G}_{co} = 500$ J m⁻², based on fracture toughness measurements of the crab exoskeleton ($K_{Ic} = 1.0 - 2.3$ MPa m^{0.5}) [33], converted to energy by the relation $\bar{G}_{co} = K_{Ic}^2/\bar{E}$ with $K_{Ic} = 2.0$ MPa m^{0.5}; (iii) constant adhesive fracture energy $G_{ad} = 75$ J m⁻², estimated as 15% of the cohesive fracture energy, roughly the ratio between the moduli of the proteinaceous matrix (1 - 1.5 GPa) [15] and \bar{E} (equation (11)); see also the biomimetic adhesive ($G_{ad} \cong 50 - 400$ J m⁻²) [34]; and (iv) laminate thickness $d = 100$ μm, similar magnitude as the scorpion cuticle thickness [16].

The intersections of the cohesive and adhesive failure stress curves in figure 3, for decreasing, homogenous and increasing moduli, are denoted by points A, B and C, respectively. At these points, crack deflection from propagation to delamination is expected, because, for a growing crack, the adhesive stress becomes lower than the cohesive stress. We see that deflection occurs much earlier (at smaller crack) when the modulus is decreasing (point A), compared to when it is homogenous (point B) or when it is increasing (point C). We take for example an initial Griffith crack of length $c = 20$ μm (the dashed vertical line), which is in the region where the cohesive stress is below the adhesive stress for all three cases. If the applied stress reaches the cohesive failure stress, the crack will propagate all the way to the deflection point, and will then deflect to delamination. This occurs at $c \cong 47$ μm for homogenous moduli and $c \cong 57$ μm for increasing moduli, most likely leading to a catastrophic failure as about half the laminate thickness ceases to contribute to the structural strength, compared to only $c \cong 23$ μm for decreasing moduli, in which case the structure may still survive.

Figure 4 maps the deflection condition as a function of the structural resilience ($R = 1 - c/d$, see definition below), the moduli grading rate for linear grading ($\Delta E/\bar{E}$) (how steeply the moduli are increasing or decreasing), and the ratio between the adhesive failure energy and the average cohesive failure energy (G_{ad}/\bar{G}_{co}). The quantities \bar{E} , G_{ad} and \bar{G}_{co} are material properties, whereas c , d and ΔE are structural properties. Using these normalized quantities makes it possible to obtain a universal plot for the deflection condition in a linearly-graded moduli case. The vertical axis in figure 4 is expressed in terms of the laminate resilience (or damage tolerance) in the presence of a crack c , here defined as

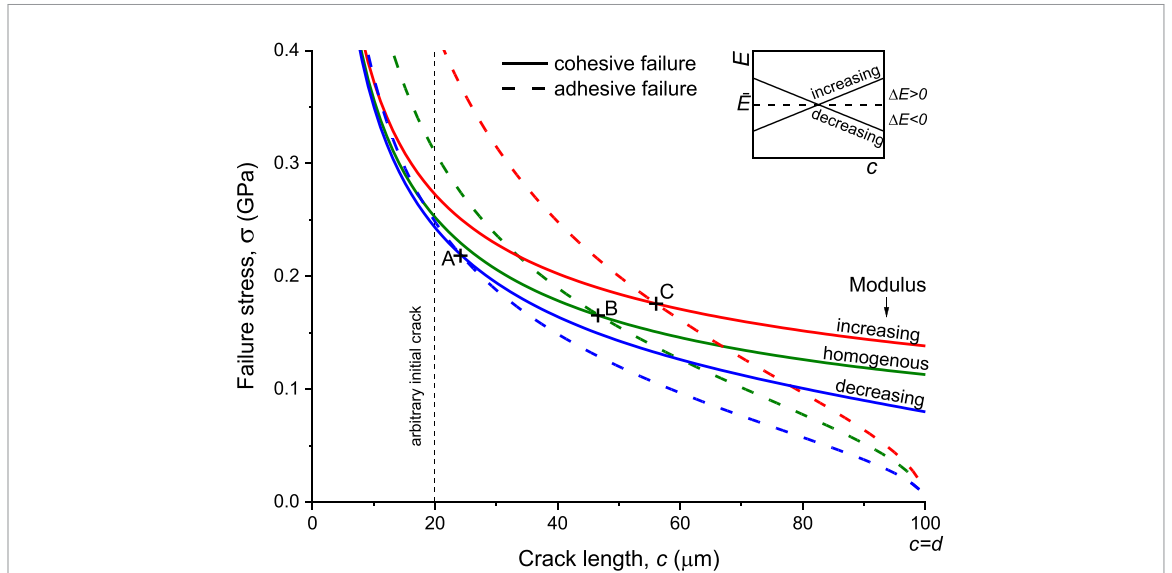


Figure 3. Cohesive and adhesive failure stresses in a laminate with linearly graded moduli. Three cases are plotted (equation (33)): (1) modulus increasing (from 4 Gpa to 12 Gpa), (2) modulus decreasing (from 12 Gpa to 4 Gpa), and (3) homogenous material with modulus of 8 Gpa. For each case, both cohesive and adhesive failure stresses are presented. The inset shows the graded moduli functions for increasing modulus ($\Delta E = 0.5\bar{E}$) and decreasing modulus ($\Delta E = -0.5\bar{E}$). Inputs: average modulus $\bar{E} = 8$ Gpa, average cohesive fracture energy $\bar{G}_{co} = 500$ J m⁻², constant adhesive fracture energy $G_{ad} = 75$ J m⁻², laminate thickness $d = 100$ μm. Points A, B and C are the deflection points from cohesive to adhesive failure for each case.

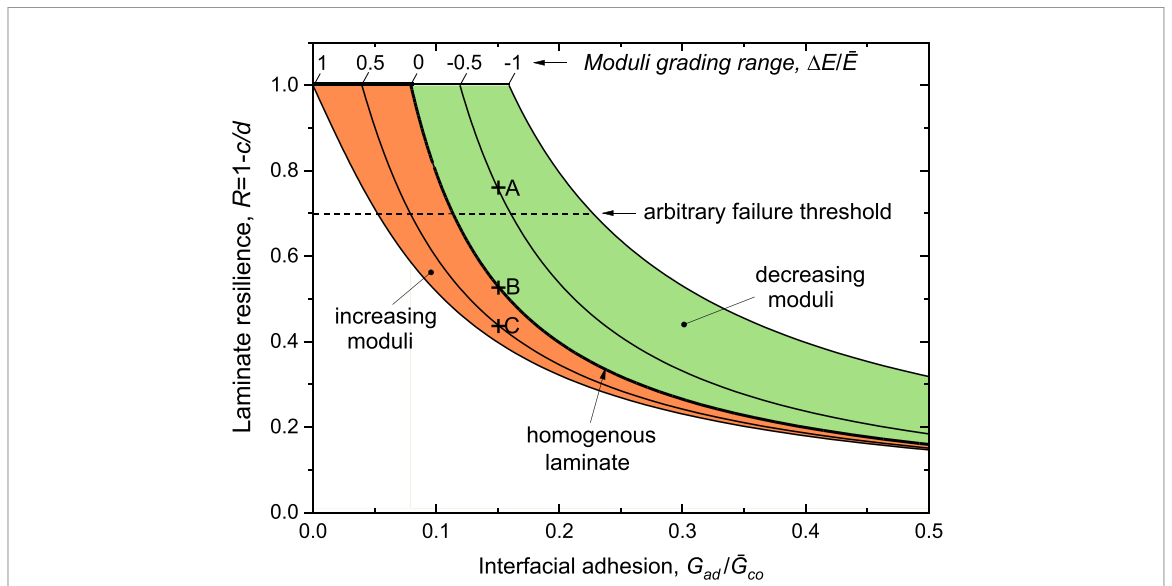


Figure 4. Resilience (relative damage tolerance) of a laminate with linearly graded moduli. Crack deflection condition expressed in terms of the resilience R (equation (35)). c is the minimal crack length required for deflection (equation (34)), normalized by the laminate thickness d . The resilience is plotted versus the interfacial adhesion fracture energy G_{ad} normalized by the average cohesive fracture energy \bar{G}_{co} . The resilience is mapped for several values of the moduli grading range ΔE , normalized by the weighted-average laminate modulus \bar{E} . The curve $\Delta E = 0$ (thick line) represents a homogenous laminate, the region left to it (orange) applies to increasing moduli (in the crack growth direction), whereas the region right to it (green) applies to decreasing moduli. Points A, B and C are examples for given $G_{ad}/\bar{G}_{co} = 0.15$ (corresponding to the same points in figure 3), demonstrating that the laminate is more resilient when the moduli are decreasing. The horizontal dashed line at $R = 0.7$ shows an arbitrary failure threshold, which expresses the minimal allowed structural resilience to avoid failure.

$$R = \frac{\sigma_{residual}}{\sigma_{strength}} = \frac{w(d-c)}{wd} = 1 - \frac{c}{d} \quad (17)$$

for a laminate with thickness d and width w . The strength $\sigma_{strength}$ is the maximum stress borne by a laminate (no flaw is present), whereas the residual strength $\sigma_{residual}$ is the stress a laminate with a crack c

can still bear without failing. In a flawless laminate the load is spread over an area wd , whereas with a crack c the load is spread over a smaller area $w(d-c)$, resulting in a stress higher by the ratio of the two areas. A higher R means that the laminate is more resilient, in other words a crack in the laminate is more likely to deflect while it is still small, and the therefore the

structure is less likely to fail catastrophically in the presence of flaws. A structure having $R = 1$ ($c = 0$) is highly resilient, whereas a structure having $R \rightarrow 0$ ($c \rightarrow d$) is weak.

In figure 4, on the left side (orange region), the layers moduli are increasing, whereas on the right side (green region) they are decreasing. Points A, B and C are the same deflection points denoted in figure 3 for decreasing, homogenous and increasing moduli, respectively. Generally, the resilience is higher (crack deflection occurs at a shorter initial crack) when the moduli grading rate is lower (smaller $(\Delta E/\bar{E})$). When the grading rate is 1 the resilience is low, improving gradually toward 0-rate where the resilience is equivalent to that of a homogenous material; below 0-rate the resilience further improves, until it reaches a maximum at a rate of -1 . The resilience is also higher when the fracture energies ratio is lower, that is lower adhesive energy and/or higher cohesive energy. The consequence of high resilience (crack deflection occurs earlier) is that the failure would likely not be catastrophic, and therefore the laminate is tougher and more reliable against a crack propagating in the direction of decreasing moduli. Conversely, if the crack would grow in the opposite direction, that of increasing layers moduli, the resilience would be lower (deflection would occur later) and the laminate might fail catastrophically. For example, given a required resilience threshold of 0.7 (horizontal dashed line), point A (decreasing moduli) is above the threshold and therefore the laminate is likely resilient, whereas point C is below the threshold (increasing moduli) and therefore the laminate is not resilient.

Observing the trends of the deflection condition in equation (7), when a crack is penetrating a progressively more compliant media (decreasing \bar{E}_2), as in the case of linearly decreasing stiffness described above, the right term of the inequality would grow, consequently increasing the possibility of deflection. At the same time, the cohesive energy at the crack tip, G_{co} , would decrease in proportion to the local modulus as the crack propagates, the result being growth of the left term as well, consequently decreasing the possibility of deflection. So, when entering a more compliant media, both sides of the deflection condition inequality increase simultaneously in competition. However, \bar{E}_2 would degrade more significantly than G_{co} , because it averages the stiffnesses in a region with progressively decreasing moduli. In other words, for a growing crack, \bar{E}_2 decreases faster than G_{co} in that condition, and the general favorable trend of the deflection criterion is maintained. By contrast, in a crack progressing into a stiffer media, as in the case of linearly increasing stiffness described above, \bar{E}_2 increases faster than G_{co} , reducing the possibility of deflection. This is indeed reflected in figure 4, which shows that when the moduli are decreasing, in other words the crack propagates into a gradually

more compliant media, the possibility of early deflection is higher compared to a crack propagating into a stiffer media.

The earlier crack deflection in a laminate with decreasing moduli comes at the cost of a lower failure stress. Supposing again the initial Griffith crack denoted by the dashed vertical line in figure 3, it intersects the cohesive failure curves at a somewhat lower stress in the decreasing moduli case, compared to the homogenous and increasing moduli cases. So, there is a trade-off between early crack deflection (the crack deflects at a lower stress) and initiation of crack growth (the crack starts propagating at a higher stress). Furthermore, although the average stiffness of the entire laminate may not be affected by graded moduli, there is a risk of a crack developing in the opposite direction, that of increasing stiffness, in which case deflection would be undesirably delayed. Thus, the application of a graded stiffness approach in synthetic laminates should be carried out carefully, ensuring that the crack growth direction can be predicted reliably. For example, laminates with one side located internally and shielded, whereas the other side exposed to external, possibly hostile, environment, can be designed with decreasing stiffness from outside to inside, to increase the probability of non-catastrophic crack deflection.

2.6. Effect of graded layers thickness

We turn now to the analysis of the effect of layer thickness, separating it from the effect of variable moduli described above by assuming uniform moduli throughout the laminate. To better understand the difference between these structural types, we observe two examples from nature: (i) a fibrous laminate, such as that of the scorpion cuticle [15, 16], which consists of soft matrix reinforced by strong chitin fibers. Such laminates have a hierarchical structure ranging from nanoscale to microscale, with matching hierarchical interfaces, and both their layer thickness and modulus vary with their location in the laminate [1]. Crack deflection can occur in any of the interfaces, even between two neighboring fibers. This structural type is described in section 3; (ii) a ceramic laminate, such as that of the sponge spicule [10–12], which consists of hard silica layers with soft thin interfacial layers. The thickness of the silica layers vary with their location in the laminate, but the modulus is uniform in all silica layers. Crack deflection can occur only at the interface between the silica layer, but not inside the silica because of its high strength. This structural type is addressed in this section.

We consider a laminate of hard layers (such as silica) having graded thicknesses, alternating with soft interfacial matrix. We assume that the tensile moduli and fracture energies of the hard layers and interfacial layers are constant throughout the laminate. In other words, the hard layers are taken as homogenous and isotropic. For the sake of simplicity we also neglect the

thickness of the thin interfacial layers. Using the laminate deflection condition of equation (15) with constant moduli and under plane stress conditions we get

$$\frac{G_{ad}}{\bar{G}_{co}} < \frac{1}{4\pi(1-c/d)} \text{ or } R = \left(4\pi \frac{G_{ad}}{\bar{G}_{co}}\right)^{-1} \quad (18)$$

where in the second equation we substituted R from equation (17). The inverse dependence of R on G_{ad} can be observed in figure 4, using the curve for a homogenous laminate (thick line) (this can be seen by substituting $\Delta E = 0$ in equation (35) used to generate this plot).

A shallow crack ($c \rightarrow 0$) would never deflect when its tip is inside a hard layer, as $G_{ad_hard} = \bar{G}_{co}$ inside an isotropic layer (the energy to break bonds is the same in all directions), whereas deflection requires that the adhesive energy be at least 4π smaller than the cohesive energy. So, a crack tip within a hard layer will likely keep propagating through the layer, until it reaches an interface where it might be deflected and bifurcate if the deflection condition is met ($G_{ad_int} \ll \bar{G}_{co}$).

Note that the deflection condition in equation (18) is independent of the modulus and the layer thickness. However, a crack starting from the face with thin layers will likely deflect at a smaller c compared to a crack starting from the face with thick layers, simply because it will quickly reach an interface.

3. Crack deflection in the scorpion cuticle

3.1. The endocuticle structure and varying stiffness

The scorpion chela's endocuticle (the inner part of the cuticle) is composed of interleaved parallel Bouligand layers and interlayers (figure 5(a), see section 5). The Bouligand layers thickness ranges from about $2.5 \mu\text{m}$ at the inner side to about $7 \mu\text{m}$ at the outer side (figure 5(b)) [1, 15, 16]. The Bouligand consists of progressively twisted and tilted laminae of unidirectional chitin-protein fibers, embedded in a proteinaceous matrix [15]. The helical laminated structure is common to all Bouligand layers, but the number of laminae comprising a single Bouligand unit is smaller in the inner layers than in the outer layers. The Bouligand resembles an angle-ply synthetic laminate, in which each lamina with fibers oriented in θ direction has a matching lamina in $-\theta$ direction. The chitin fibers in a lamina are held together by the matrix, protein partially reinforced by metal ions and chitin fragments, and the laminae are bonded together by the same matrix, in similarity to synthetic composites. However, unlike artificial laminates, the laminae in the scorpion Bouligand are tilted out of the main plane, and are rotated around their edges and not centers, making the structure highly asymmetrical and warped (figure 6). Refer to description in [15].

The tilting rotation of laminae induces an angular gap between adjacent laminae, which effectively reduces the fiber volume fraction in a Bouligand. This gap is larger in the Bouligands close to the inner side of the endocuticle (figure 6(a)), and smaller in those near the outer side (figure 6(b)); this is because the inner Bouligands have less laminae than the outer ones, while the tilting range of both is the same, -90° to $+90^\circ$. The mean effect of tilting on the fiber volume fraction V_f , estimated in 'Fiber volume fraction in a Bouligand' in the appendix, is:

$$V_f \cong \frac{\pi}{4} \left[1 + \frac{\pi/2}{t/w - 2}\right]^{-1} \quad (19)$$

where t is the total height of a Bouligand, and w is its lamina width. Thus, the fibers mean volume fraction depends nonlinearly on the Bouligand's aspect ratio t/w (height over width): The higher the aspect ratio, the higher the volume fraction, and vice versa. Consequently, the endocuticle outer Bouligand layers are considerably stiffer than the inner layers. This observation is confirmed by detailed laminate stiffness analysis of Bouligand units with varying height (see section 5) [15], and is depicted in figure 6(e), along with the corresponding fiber mean volume fraction. From outside the endocuticle to its inside, the Bouligand moduli degrade from about 10 GPa to 4 GPa in the x -direction, and from about 7 GPa to 3 GPa in the y -direction. The fiber mean volume fraction degrades in a similar way from about 55% to 25%.

The Bouligand layers are separated by thin interlayers of unidirectional chitin fibers oriented along the y axis, embedded in a proteinaceous matrix. The interlayers have variable thickness as well, ranging from about $1.14 \mu\text{m}$ at the inner side of the endocuticle to about $2.08 \mu\text{m}$ at the outer side (figure 5(b)) [1, 15, 16]. The interlayers moduli calculated by laminate analysis, assuming perfect fiber alignment with the y axis, are 41 GPa in the y direction (chitin fibers direction) and 3.3 GPa in the x direction [15]. These values are adjusted to 15 GPa and 5 GPa, respectively, to accommodate for: (i) the deviation from perfect fiber alignment as seen in TEM imaging of interlayers, and (ii) the in-plane isotropic moduli observed by nanoindentation and bending tests of the endocuticle layer [15, 16].

The variation of moduli across the endocuticle thickness is depicted in figure 7, demonstrating the abrupt changes between alternating Bouligand layers and interlayers. Unlike the Bouligand layers, the interlayers moduli do not vary with respect to their z -position in the cuticle, even though their thickness does vary, as their fiber volume fraction and orientation are uniform; this is reflected in the narrow peaks in figure 7. The moving average of the moduli in the x -direction, E_x (dashed line), shows a significant nonlinear degradation of the moduli with

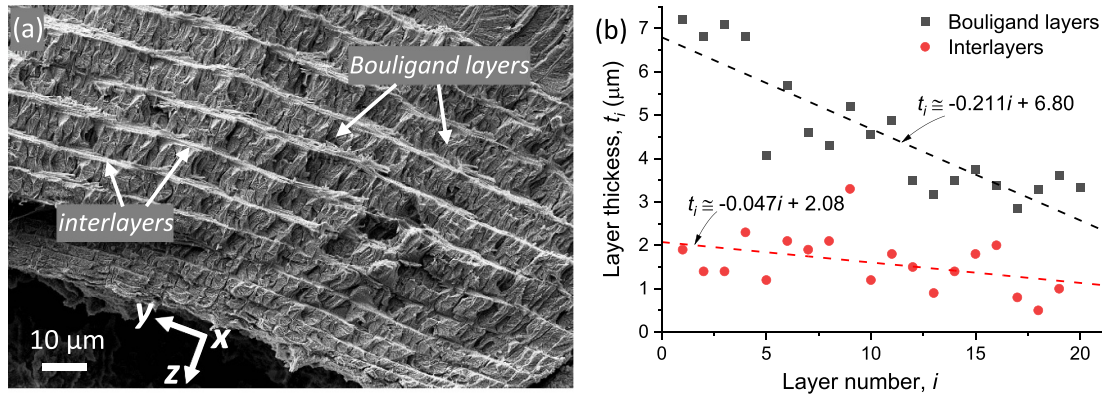


Figure 5. Bouligand layers and interlayers in the scorpion’s endocuticle. (a) SEM picture of an endocuticle cross-section, showing Bouligand layers and interlayers with varying thickness. The layers are parallel to the xy plane (x is perpendicular to the image plane). (b) Thickness data of Bouligand layers and interlayers versus the layer number from the endocuticle top (external surface), with linear fits. [Plot adapted from [1].]

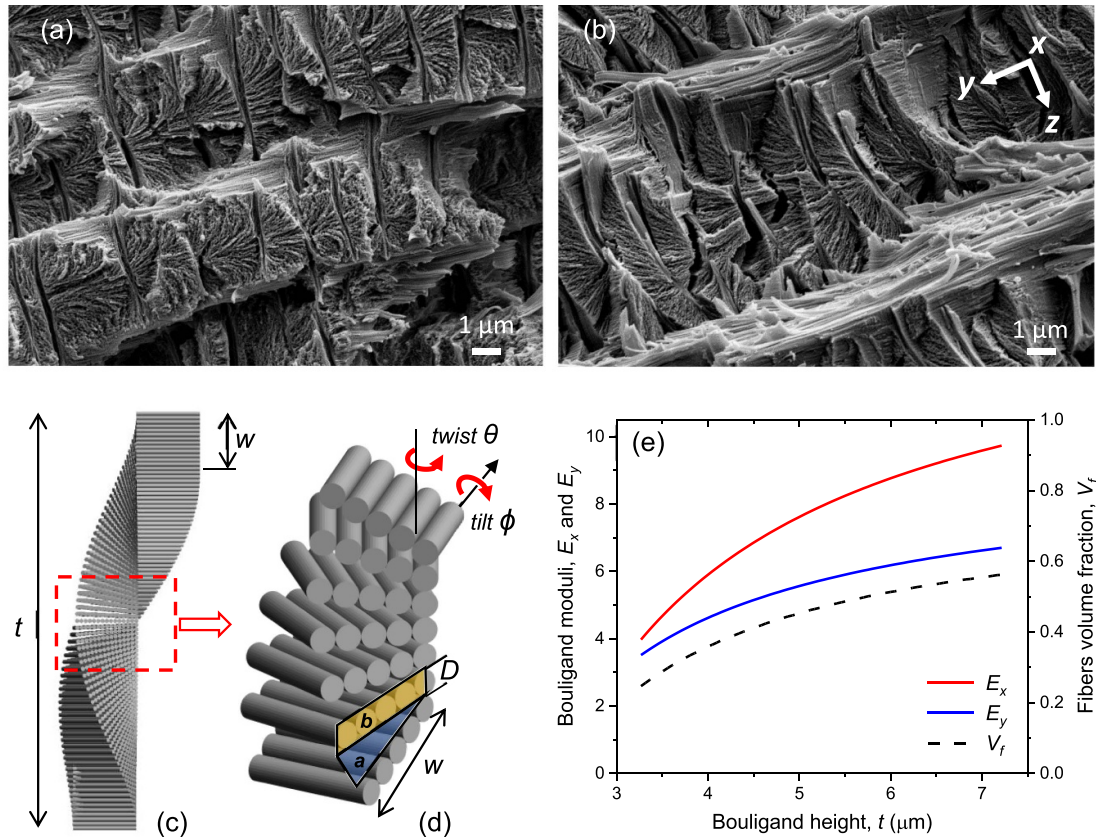
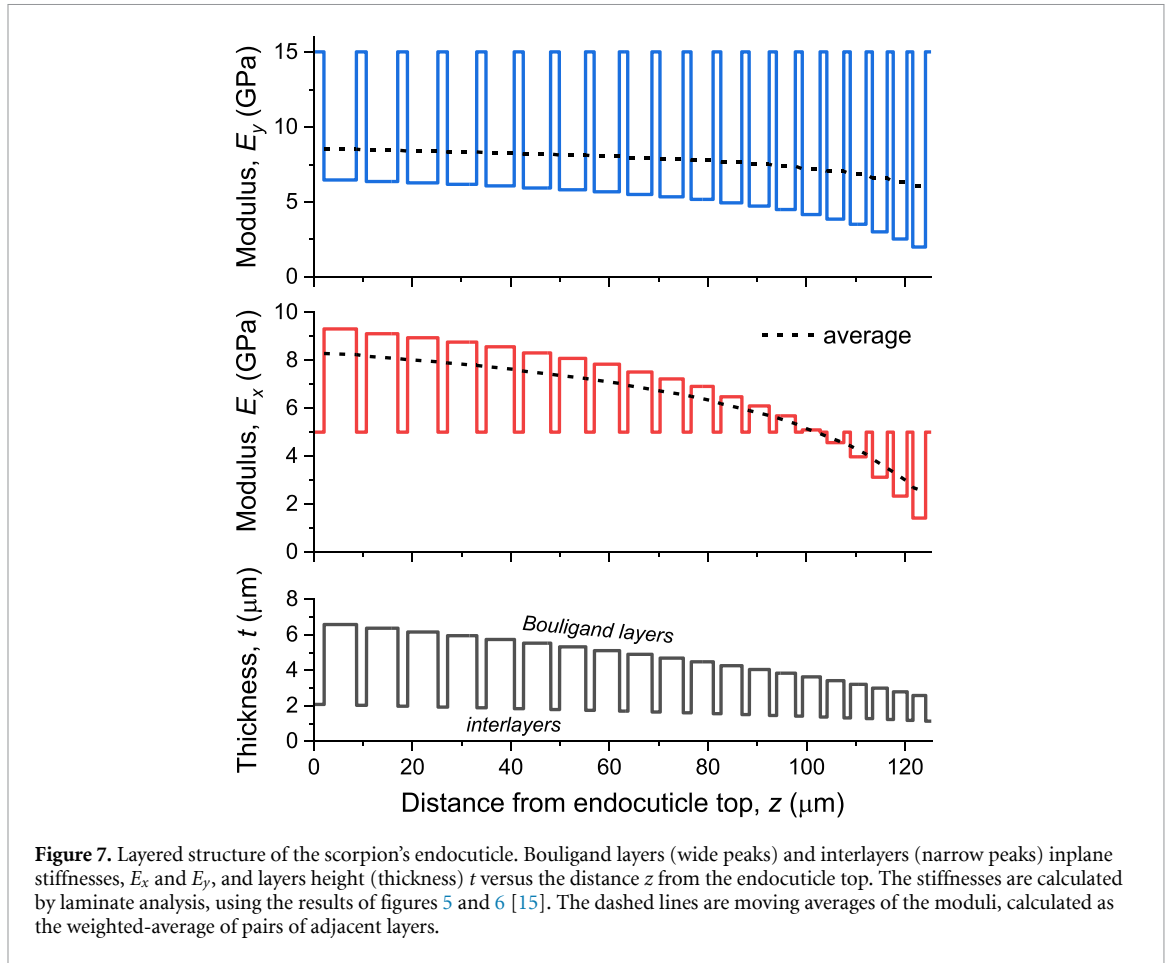


Figure 6. Bouligand laminated structure and elastic moduli. (a) SEM pictures of Bouligand morphology at the inner side of the endocuticle and, (b) at the outer side of the endocuticle. (c) Model of the Bouligand laminate [15]. (d) Laminae twist and tilt angular rotations, and definition of lamina cross sectional area b and inter-laminae gap area a . (e) Bouligand elastic moduli, and fiber mean volume fraction, vs. the Bouligand height, calculated by laminate analysis [15]. Inputs: number of laminae in a Bouligand (range) $m = [19..100]$, twisting and tilting angular ranges $\phi = [-90^\circ, +90^\circ]$, lamina width $w = 1.2 \mu\text{m}$, fiber and lamina thickness $D = 49 \text{ nm}$.

the distance from the endocuticle top (from 8.3 GPa to 2.5 GPa), because the modulus of the Bouligand layers (wide peaks) is dominant over the modulus of the interlayers (narrow peaks) in that direction.

By comparison, in the y -direction, E_y moderately degrades nonlinearly (from 8.5 GPa to 6.1 GPa), because of the dominance of the interlayers’ moduli in that direction.



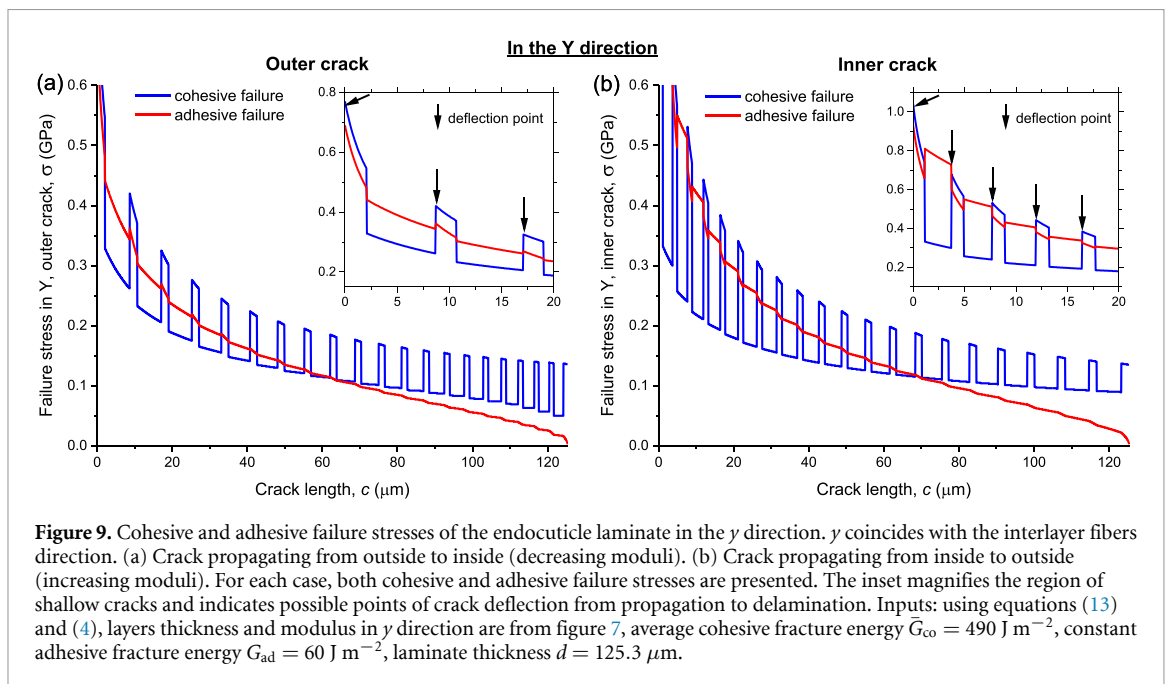
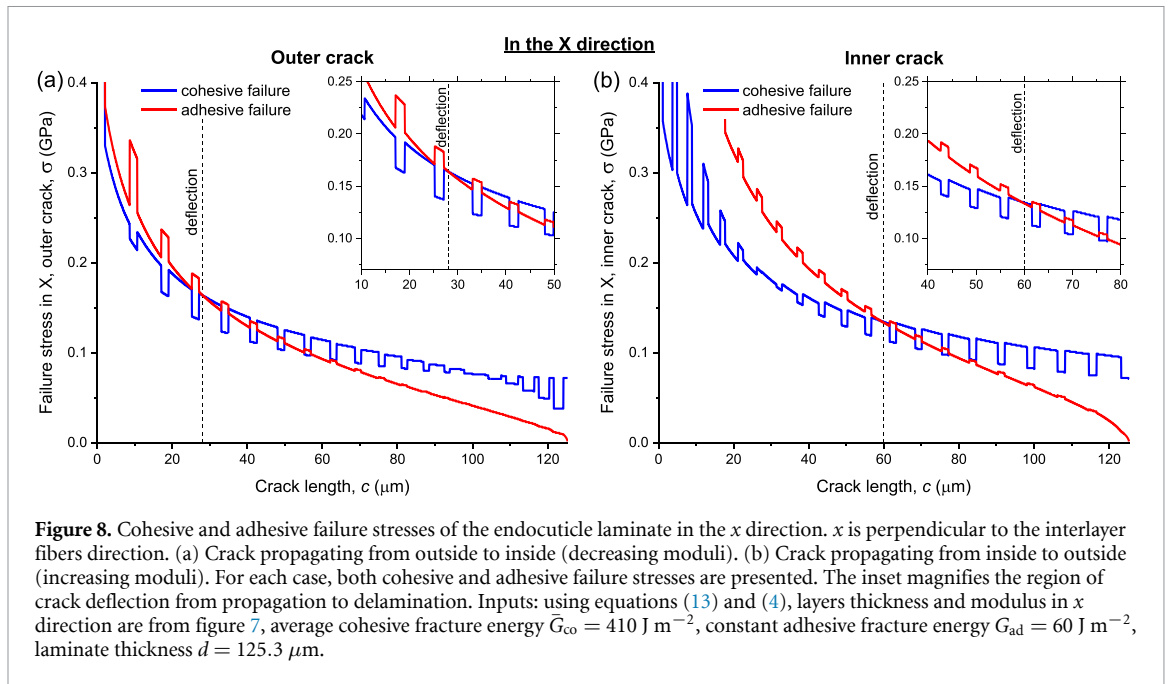
3.2. Failure stresses and crack deflection in the endocuticle

The calculated cohesive and adhesive failure stresses in the endocuticle in the x and y directions (equations (13) and (4)), as functions of the crack length, are presented in figures 8 and 9, respectively. The following endocuticle material data was used to generate these plots: (i) measured layers thickness and calculated moduli (figure 7); (ii) average cohesive fracture energies $\bar{G}_{co,x} = 410 \text{ J m}^{-2}$ and $\bar{G}_{co,y} = 490 \text{ J m}^{-2}$, based on 500 J m^{-2} (section 2.4) adjusted for the average modulus in each direction, \bar{E}_x and \bar{E}_y . (iii) Constant adhesive fracture energy of the proteinaceous matrix, $G_{ad} = 60 \text{ J m}^{-2}$, estimated as $\sim 15\%$ of the cohesive energy (section 2.4); and (iv) laminate thickness $d = 125.3 \mu\text{m}$ (figure 7). The endocuticle laminate is approximated as brittle, a state comparable to the dehydrated cuticle samples investigated in our scorpion studies [15, 16].

We observe the evolution of the failure stresses for loading in two directions: (i) the x direction (figure 8), which is the direction perpendicular to the fibers in an interlayer (perpendicular to the image-plane in figures 5(a) and 6(a), (b)); and (ii) the y direction (figure 9), which is the direction coincident with the fibers in an interlayer (in the image-plane in figures 5(a) and 6(a), (b)). In each loading case, the surface of the propagating crack is

perpendicular to the loading axis. The general trends are similar to those in the linearly graded moduli example (figure 3), in that a propagating crack reaching the deflection point (the cross section between the cohesive and adhesive curves), will deflect to a delamination crack because the adhesive failure stress becomes lower than the cohesive failure stress. Furthermore, when the crack starts at the endocuticle outer boundary, its deflection will occur much earlier (for example, $c \cong 28 \mu\text{m}$ in figure 8(a)) than a crack starting at the inner boundary (for example, $c \cong 60 \mu\text{m}$ in figure 8(b)), making the structure more reliable against external cracks. The corresponding structural resilience is $R \cong 0.78$ and $R \cong 0.52$, respectively, compared to $R \cong 0.54$ for a homogenous laminate having the same fracture energies (equation (18)).

The analysis above was carried out for the dry, brittle state of the endocuticle. In nature, the cuticle contains moist which acts as a plasticizer, making the cuticle less stiff and more plastic, causing it to fail at a lower stress and with a much larger deformation [16]. This, however, should have low impact on the crack deflection condition, as expressed in equation (7). The ratio of fracture energies G_{ad}/G_{co} will likely remain similar to the dry state, because the added plasticity in the wet state may increase the adhesive and cohesive energies in a similar way. Likewise, the ratio of moduli \bar{E}/\bar{E}_2 will likely remain similar



to the dry state, because the reduced stiffness in the wet state should decrease the average moduli in different parts of the laminate by the same proportion. Thus, the point of crack deflection, that is the length of a Griffith crack at which deflection occurs, should be similar in both dry and wet states. Bending tests of cuticle samples demonstrated similar delamination phenomena in dry and wet conditions, supporting this deduction [16].

3.3. Complex fracture paths through the endocuticle

The most noticeable feature in the stress plots in figures 8 and 9 are the fluctuations of the failure

stresses, caused by the dissimilar moduli and cohesive fracture energies between a Bouligand layer (wide peaks) and an interlayer (narrow peaks). Such fluctuations may induce peculiar structural behavior, resulting in complex fracture paths through the endocuticle. How do we know what will be the preferred path selected by the crack? Basically, as described previously, the preferred path will be determined by the cohesive and adhesive fracture stresses, such that the path driven by the lower stress will be favored, whether propagation or delamination. Because of the significant stress fluctuations in the cuticle, the preferred path may alternate between the two crack

For example, in the x direction, a cohesive failure in figure 8(b), for a crack whose tip is at a Bouligand layer (a negative wide peak at say $c = 10 \mu\text{m}$), might be arrested when reaching the neighboring interlayer (a positive narrow peak), because it requires a much higher stress for propagation; however, a larger initial crack (say $c > 30 \mu\text{m}$) whose tip is at an interlayer (a negative narrow peak), might be arrested when reaching a neighboring Bouligand layer (a positive wide peak). These fluctuations may even cause a delamination crack to revert back to a propagating crack. For example, considering a delamination crack whose tip is at the Bouligand layer at the deflection point in figure 8(a), if a Griffith defect a few microns deep is encountered in the neighboring interlayer, the stress required for a cohesive failure is about half that of the adhesive stress, and the crack might revert back to propagation (the stress threshold is a factor of 2, see last para. in section 2.3). A probable initial Griffith defect may be the weak interface in the z -direction between adjacent Bouligands (the intralayer [15]).

In the y direction (figure 9), the scenario is quite different, because of the large gap between the high interlayer stiffness (the positive narrow peaks) compared to the low Bouligand stiffness in this direction (figure 7). As the interlayer cohesive stress peaks are always above the adhesive stress, for any given Griffith crack, a propagating crack whose tip is at an interlayer will always deflect. Similarly, a propagating crack whose tip is at a Bouligand layer (a negative wide peak) will always deflect once it encounters an interlayer. This may occur for very shallow cracks, in both the inner and outer crack scenario, as the peaks of the cohesive failure stress (blue curves in figure 9) are always higher than the adhesive failure stress (red curves). Possible deflection points, the occurrence of which depends on the length of the initial crack, are indicated by arrows, demonstrating that the structural resilience in that direction is very high (close to 1). Diversion from delamination back to propagation may also occur in a shallow inner crack (for example, $c = 7 \mu\text{m}$ in figure 9(b)), where a possible defect in a Bouligand layer might initiate a Griffith propagating crack because of a much lower (by a factor of ~ 2) cohesive stress than adhesive stress.

In summary, two complementary crack diversion mechanisms are active in the endocuticle structure: decreasing modulus, which is predominant in the x direction, and fluctuating modulus, which is predominant in the y direction. In both mechanisms, cracks are diverted when the applied stress needed for delamination is lower than that required for propagation. However, the two mechanisms act differently: decreasing modulus relies on the average stiffness of large regions that release and gain elastic energy as a result of crack propagation, whereas fluctuating modulus relies on the stiffness variations near the crack tip. In other words, decreasing modulus

depends mostly on global properties, whereas fluctuating modulus depends mostly on local properties. Both mechanisms significantly enhance the structural resilience with respect to a laminate with uniform modulus.

3.4. Experimental evidence

The benefit from the proposed crack deflection model is the ability to investigate different scenarios of loading, laminate configuration, and material properties. Probing the structure of the scorpion's cuticle at nano and micro scale to track the evolution of cracks across layers is very challenging and beyond the scope of this study. However, macroscale mechanical tests carried out in previous studies provide some supporting evidence for the model. These include: (i) nanoindentation tests at the cuticle cross-section in both directions [17], and (ii) bending tests of cuticle strip samples in both directions [16].

In the nanoindentation tests, the nanoindenter presses a diamond tip against the tested sample, allowing calculation of the modulus from the force-displacement curve and hardness from the dent depth at maximum force. The results of the moduli at the upper region of the endocuticle were $E_x = 8.5 \text{ GPa}$ and $E_y = 8.2 \text{ GPa}$ (dry samples) [17], in agreement with the calculated average moduli in figure 7. These measurements are averages taken at 30 random points on the endocuticle, covering both Bouligands and interlayers. To isolate the moduli of the standalone Bouligand, the stiffness of the interlayer was separated, resulting in Bouligand moduli of $E_x = 9.6 \text{ GPa}$ and $E_y = 6.6 \text{ GPa}$ [15], in agreement with the calculated average moduli in figure 6(e).

Quasi-static three-point bending tests were carried out, providing the flexural modulus, stiffness, strength, and toughness. The measured moduli were $E_x = 11.1 \text{ GPa}$ and $E_y = 7.3 \text{ GPa}$ (dry samples) [16], similar to the nanoindentation results (considering the different testing method and the added impact of the other cuticle layers). The corresponding measured strength was $\sigma_x = 270 \text{ MPa}$ and $\sigma_y = 210 \text{ MPa}$ (dry samples), which, according to the analysis in figure 8 in the x direction and figure 9 in the y direction (for an outer crack), would initiate a cohesive failure at an initial crack of size $\sim 10 \mu\text{m}$. This small predicted critical crack size, representative of common defects on the outer side of the cuticle, indicates that the actual failure might indeed be caused by crack propagation, rather than by exceeding the ultimate strength. Furthermore, the measured plastic work to fracture was $\sigma_x = 1.1 \text{ mJ mm}^{-2}$ and $\sigma_y = 0.7 \text{ mJ mm}^{-2}$, likely implying higher energy dissipation in the x direction due to delamination as a result of an early crack deflection, as shown in figure 8.

The result in figure 8, deflection at a relative Griffith crack length of $c/d = 0.22$, is also in agreement with the observed experimental fracture

patterns [16], seen in figure 1 as well. These show a delamination crack appearing at a typical relative crack length of $c/d = 0.25 \pm 0.05$, demonstrating that deflection indeed occurs fairly close to the external boundary. The experimental results are also in agreement with the crack deflection predictions presented in the example in figure 3 for a laminate with linearly decreasing moduli ($c/d = 0.23$), which uses material properties similar to the scorpion (except for the absence of the unidirectional interlayers). Finally, the experimental fracture patterns exhibit a characteristic diffused damage, with multiple randomly distributed cracks over a fairly large region, attesting to the complex predicted fracture paths described in the previous section.

4. Conclusions

Laminated structures are common in biology, consisting of layers of strong and stiff materials with soft interfaces. The layers are often nonuniform, as in the scorpion's exoskeleton where both the thickness and stiffness are decreasing from outside to inside. A key question is whether such graded properties confer structural advantages to the animal, which could be used as inspiration in engineering laminates. The present study offers an answer to this intriguing question, showing that the structural resilience against fracture is indeed affected by graded layer properties which, in specific cases, lead to early crack arrest. A new generalized multi-layer, multi-material analytical model for crack deflection in layered configurations is proposed, which describes the sometimes counter-intuitive consequences on structures with graded stiffness and thickness.

The conditions for crack instability in a laminate with variable laminae thickness and stiffness are modeled, using linear elastic fracture mechanics. Two crack types are analyzed: a Griffith crack (cohesive failure), and a delamination crack (adhesive failure), both under a tensile load. Of interest is the occurrence of deflection from the first type to the second, which occurs when the adhesive failure stress becomes lower than the cohesive failure stress as the crack propagates. Such deflection avoids catastrophic cracking failure by diverting the crack, hence making the laminate more resilient. The model is applied to the structure of the scorpion cuticle, a natural example of a laminate with variable stiffness and thickness across its layers.

The study shows that a crack propagating in a direction of decreasing stiffness, will be deflected sooner, while still small, than a crack propagating in a direction of increasing stiffness. This result seems counter-intuitive at first glance, as a propagating crack should find it easy to enter compliant media (decreasing stiffness), but, because delamination is even easier when entering such compliant media, the net result is higher tendency for crack deflection. The reason

for this is the difference in the way the elastic strain energy is released and gained during propagation or delamination.

The advantage of such graded stiffness is demonstrated by calculation with the scorpion cuticle, which has decreasing stiffness and thickness from outside (the side exposed to the environment) to inside, making it less vulnerable to external cracks induced by its harsh living conditions. In other words, the endocuticle structure 'sacrifices' the endurance against inner cracks in favor of endurance against outer cracks, which are more common because the exoskeleton is directly in contact with the environment. The cuticle's unique combination of quasi-isotropic Bouligand layers and anisotropic interlayers causes abrupt fluctuations in the failure stresses, which act to arrest and deflect propagating cracks. Synthetic man-made structures may benefit from this biological example, by incorporating graded moduli and stiffness fluctuations in the design.

5. Materials and methods

5.1. Scanning electron microscopy (SEM)

The cuticle samples were fixated with 2% glutaraldehyde and 3% paraformaldehyde in 0.1 M cacodylate buffer (pH 7.3) for 12 h at 4 °C, then for additional 3 d in a fresh buffer, and finally rinsed with 0.1 M cacodylate for 10 min three times. Post-fixation was carried out for 1 h with 1% OsO₄ in 0.1 M cacodylate buffer at room temperature, and then the samples were washed with 0.1 M cacodylate buffer, dehydrated using graded-concentration ethanol, and dried in a critical point drying machine (Baltech CPD 030). The samples were manually broken to expose cross-sections of interest, and coated by gold-palladium alloy using an Edwards (Sanborn, NY) S150 sputter. SUPRA-55 VP and Sigma 500 (Zeiss, Oberkochen, Germany) microscopes with a secondary electron (SE2) detector obtained the high-resolution SEM (HRSEM) imagery, at 5 kV acceleration voltage and 14–15 mm distance. The Bouligand dimensions and the layers count and thickness were measured from the SEM images by ImageJ [17].

5.2. Bouligand stiffness modeling

Laminate theory enables analysis of the elastic deformation under load of a laminate consisting of parallel laminae (layers) arbitrarily arranged. The stiffness of the helical structure of the Bouligand was modeled by classical laminate theory [35], with modification to reflect the effect of lamina tilting, which results in non-parallel laminae and hence non-uniform stress in a lamina. To resolve this non-uniformity, each tilted lamina was broken down to discrete sub-laminae, each parallel to the Bouligand midplane and having uniform stress depending on its distance from the midplane. Integration of the stiffness components along each lamina yielded new

tilting terms in the laminate stiffness matrices, which depend on the number of laminae in each Bouligand, derived from the SEM imagery [15].

Data availability statement

All data that support the findings of this study are included within the article.

Acknowledgments

Thanks are due to our former colleague Dr Israel Kellersztein (currently a postdoctoral scholar at Caltech), for his extensive pioneering research on scorpions. The authors would like to acknowledge support from the GMJ Schmidt Minerva Centre of Supramolecular Architectures at the Weizmann Institute, and the generosity of the Harold Perlman family. HDW is the incumbent of the Livio Norzi Professorial Chair in Materials Science.

Conflict of interest

The authors declare no conflict of interest.

Funding

This research received no external funding.

Appendix. Cohesive and adhesive failure stresses

Anisotropic inhomogeneous plate

A laminate is a special case of a continuously anisotropic inhomogeneous plate. We start with the general case of an anisotropic inhomogeneous plate, and then apply its solution to a laminate. The structure of a laminate is discrete, as it consists of distinctly separate laminae, each with different thickness and mechanical properties. Thus, to obtain the solution for a laminate, we discretize the plate solution by converting it from the continuous space to an equivalent discrete space.

Consider a plate of thickness d and width w (figure 10), infinite in the x direction, made of a continuously anisotropic inhomogeneous material whose mechanical properties—stiffness $E(z)$, cohesive fracture energy $G_{co}(z)$, and adhesive fracture energy $G_{ad}(z)$ —vary as a function of the depth z (inhomogeneity). The plate is subjected to uniform in-plane stress σ in the x direction. A Griffith crack of length c , perpendicular to the loading direction, propagates towards an interface, and can either proceed in a self-similar fashion or deflect perpendicularly along a length l within the interface. The plate mechanical properties are anisotropic within the xy plane, and therefore vary with respect to a given loading direction.

Cohesive failure

The elastic energy released by a crack c in the triangular region with base $2\pi c$ and height c (figure 10, red region), per unit width w of the plate, is given by integrating the elastic energy density $\frac{1}{2}\varepsilon^2 E(z)$ over the area $A = \pi c^2$

$$U_e = \frac{1}{2} \int_0^c \varepsilon^2 E(z) dA \quad (20)$$

where $\varepsilon = \sigma/\bar{E}$ is the strain, assumed uniform throughout the plate (prior to cracking), so that it can be taken out of the integration. $\bar{E} = (1/d) \int_0^d E(z) dz$ is the plate's average in-plane stiffness, independent of c . The triangular region is an approximate representation of the region where stress is released upon crack advancement (assuming relatively small c/d), commonly used to simplify the more elaborate solution from the theory of elasticity [36–38]. It is also assumed that the elastic energy gained outside the triangular region after cracking is negligible, so that the overall strain remains unchanged and negligible work is done by the applied stress. The area element dA (depicted in figure 10) in the triangular region is $dA = 2\pi(c-z)dz$. The elastic energy is then

$$U_e = \frac{\pi \sigma^2}{\bar{E}^2} \int_0^c (c-z) E(z) dz. \quad (21)$$

For a propagating crack (cohesive failure), the surface energy gained by the crack, per unit width, can also vary as function of the depth, and is therefore obtained by

$$U_s = \int_0^c G_{co}(z) dz \quad (22)$$

where $G_{co}(z)$ is the fracture energy at depth z .

The rates of change of these energies with a growing crack are obtained by differentiating the energies with respect to c

$$\begin{aligned} \frac{\partial U_e}{\partial c} &= \frac{\pi \sigma^2}{\bar{E}^2} \frac{\partial}{\partial c} \int_0^c (c-z) E(z) dz \\ &= \frac{\pi \sigma^2}{\bar{E}^2} \int_0^c E(z) dz = \frac{\pi \sigma^2 c \bar{E}_1}{\bar{E}^2} \end{aligned} \quad (23)$$

where $\bar{E}_1 = (1/c) \int_0^c E(z) dz$ is the average stiffness in the plate upper region, and

$$\frac{\partial U_s}{\partial c} = \frac{\partial}{\partial c} \int_0^c G_{co}(z) dz = G_{co}(c) = G_{co} \quad (24)$$

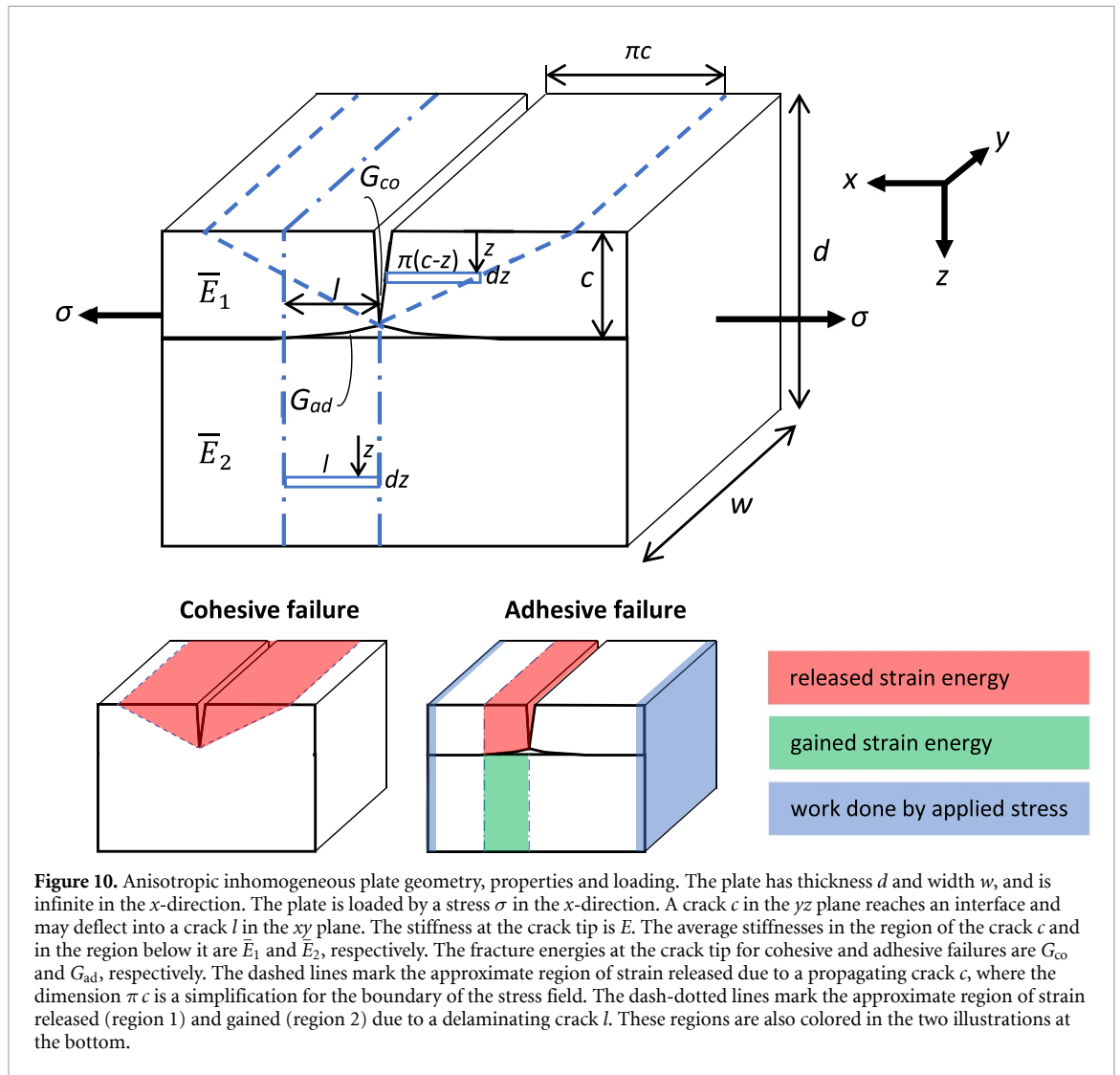


Figure 10. Anisotropic inhomogeneous plate geometry, properties and loading. The plate has thickness d and width w , and is infinite in the x -direction. The plate is loaded by a stress σ in the x -direction. A crack c in the yz plane reaches an interface and may deflect into a crack l in the xy plane. The stiffness at the crack tip is E . The average stiffnesses in the region of the crack c and in the region below it are \bar{E}_1 and \bar{E}_2 , respectively. The fracture energies at the crack tip for cohesive and adhesive failures are G_{co} and G_{ad} , respectively. The dashed lines mark the approximate region of strain released due to a propagating crack c , where the dimension πc is a simplification for the boundary of the stress field. The dash-dotted lines mark the approximate region of strain released (region 1) and gained (region 2) due to a delaminating crack l . These regions are also colored in the two illustrations at the bottom.

where G_{co} is the cohesive fracture energy at the crack tip. Both derivatives are functions of c , but depend on it differently: the energy G_{co} is defined at a specific location—the crack tip ($z = c$), whereas the stiffness \bar{E}_1 is defined as an average over the entire upper region ($z = [0, c]$).

The condition for crack instability, that is, propagation, is obtained by equating the energy rates of equations (23) and (24). Thus, the stress causing further propagation of the crack (cohesive failure), $\sigma = \sigma_{co}$, is

$$\sigma_{co} = \bar{E} \left[\frac{G_{co}}{\pi c \bar{E}_1 (1 - \nu^2)} \right]^{1/2} \quad (25)$$

This is equation (1). Also added in this equation is the term $1 - \nu^2$ for the effect of Poisson's ratio in plane strain condition; in plane stress condition, for example in a thin plate such as the scorpion's cuticle, this term is removed.

Adhesive failure

The elastic energy released by the crack l in the approximate rectangular region cl (figure 10, red region), per unit width w of the plate, is given by integrating the elastic energy density $\frac{1}{2} \varepsilon_1^2 E(z)$ over the area $A = cl$

$$U_{e1} = \frac{1}{2} \int_0^c \varepsilon_1^2 E(z) dA = \frac{1}{2} \varepsilon_1^2 l \int_0^c E(z) dz = \frac{1}{2} \varepsilon_1^2 l c \bar{E}_1 \quad (26)$$

where $\varepsilon_1 = \sigma / \bar{E}$ is the strain, assumed uniform throughout the rectangular region (prior to cracking), so that it can be taken out of the integration. As before, $\bar{E} = (1/d) \int_0^d E(z) dz$ is the plate's average in-plane stiffness, and $\bar{E}_1 = (1/c) \int_0^c E(z) dz$ is the average stiffness in the upper region. The area element dA (depicted in figure 10) in the rectangular region is $dA = l dz$. Similarly, the elastic energy gained in the rectangular region $A = (d - c)l$ (green region) is

$$U_{e2} = \frac{1}{2} \int_c^d (\varepsilon_2^2 - \varepsilon_1^2) E(z) dA = \frac{1}{2} (\varepsilon_2^2 - \varepsilon_1^2) l(d-c) \bar{E}_2 \tag{27}$$

where $\varepsilon_2 = [\sigma / (1 - c/d)] / \bar{E}_2$ is the strain, assumed uniform throughout this rectangular region, where the stress was augmented by the factor $d / (d - c)$ because the full load is now applied on a smaller cross section $d - c$. $\bar{E}_2 = 1 / (d - c) \int_c^d E(z) dz$ is the region's average in-plane stiffness, a function of c . The surface energy gained by the crack is given by

$$U_s = lG_{ad}(c) = lG_{ad} \tag{28}$$

where G_{ad} is the adhesive fracture energy for a delamination crack at the interface touched by the crack tip. The work done by the stress (blue region) is given by

$$w = (\varepsilon_2 - \varepsilon_1) l \sigma d \tag{29}$$

where $(\varepsilon_2 - \varepsilon_1) l$ is the net elongation of the plate, and σd is the tensile force per unit width of the plate.

To obtain the condition for crack instability, that is, delamination, the sum of the rates of change of these energies with a growing crack, obtained by differentiating the energies in equations (26)–(29) by l , should have a zero net change

$$\frac{1}{2} \varepsilon_1^2 c \bar{E}_1 - \frac{1}{2} (\varepsilon_2^2 - \varepsilon_1^2) (d - c) \bar{E}_2 - G_{ad} + (\varepsilon_2 - \varepsilon_1) \sigma d = 0. \tag{30}$$

Note that, in this equation, released energy and work terms have a positive sign, whereas gained energy and fracture energy terms have a negative sign. Substituting ε_1 and ε_2 , and solving for the stress causing a delamination crack (adhesive failure), $\sigma = \sigma_{ad}$, we get

$$\sigma_{ad} = \left[\frac{2G_{ad}\bar{E}}{c} \left(1 - \frac{c}{d} \right) \frac{\bar{E}_2}{\bar{E}_1} \right]^{1/2} \tag{31}$$

This is equation (3).

In this analysis, we assumed that the strain energy U_{e1} in the rectangular region cl is completely released and adds up to the growth of the delamination crack. However, when a Griffith crack moving at some speed deflects perpendicularly, a new delamination crack initiates from a stationary state and starts accelerating. Thus, at the early stage of delamination, some strain energy is still stored in this region [18, 28, 30]. As a rough approximation, we assume that this energy is zero near the Griffith crack (an unstrained free end), and increases linearly toward the delamination crack tip, reaching the value of equation (26) at distance l , where the strain is ε_1 . Integrating the energy

over that region, $\frac{1}{l} \int_0^l (U_{e1} \frac{x}{l}) dx = \frac{1}{2} U_{e1}$, the total released energy would be reduced by a factor of 2. Substituting this approximation in equation (30), and recalculating the adhesive fracture stress at delamination initiation, a factor of $\sqrt{2}$ should be added to equation (31) when used for the crack deflection condition (see section 2.3).

Discretization of average stiffnesses

The average stiffnesses \bar{E} , \bar{E}_1 and \bar{E}_2 are obtained by integrating the tensile moduli along the z -axis, over the respective ranges. A laminate is a special case of a continuously anisotropic inhomogeneous plate, where the plate is divided into multiple laminae, each with its own uniform stiffness in the loading direction. Thus, the stresses for cohesive and adhesive failures in a laminate can be obtained by discretizing the anisotropic inhomogeneous plate expressions (equations (25) and (31)).

Consider a discrete laminate, made of successive laminae numbered $i = [1..n]$, each of thickness t_i and stiffness E_i in the loading direction, penetrated by a Griffith crack of length c , whose tip reaches inside lamina k . The distance from the crack tip to the bottom boundary of lamina k is $\sum_{i=1}^k t_i - c$ and to its top boundary is $\sum_{i=k}^n t_i - (d - c)$ (figure 2). These distances are used for splitting the weighted contribution of lamina k modulus, E_k , between \bar{E}_1 and \bar{E}_2 . Discretizing the integrals, the laminate average stiffnesses are obtained:

$$\begin{aligned} \bar{E} &= \frac{1}{d} \int_0^d E(z) dz = \frac{1}{d} \sum_{i=1}^n E_i t_i \\ \bar{E}_1 &= \frac{1}{c} \int_0^c E(z) dz = \frac{1}{c} \left[\sum_{i=1}^k E_i t_i - E_k \left(\sum_{i=1}^k t_i - c \right) \right] \\ \bar{E}_2 &= \frac{1}{d-c} \int_c^d E(z) dz \\ &= \frac{1}{d-c} \left[\sum_{i=k}^n E_i t_i - E_k \left(\sum_{i=k}^n t_i - d + c \right) \right]. \tag{32} \end{aligned}$$

Linearly graded moduli

Consider a laminate with linearly graded modulus of the form specified in equation (16). The calculation of the average moduli in the laminate upper part ($z < c$) and lower part ($z > c$) yields (using equation (32)) $\bar{E}_1 = \bar{E} + (c/d - 1) \Delta E$ and $\bar{E}_2 = \bar{E} + (c/d) \Delta E$, respectively, where \bar{E} is the weighted-average stiffness of the entire laminate, and ΔE is the moduli grading range. For simplicity, we assume very thin

laminae of uniform thickness, so that the equations for a continuously anisotropic inhomogeneous plate may be used as approximation. The local cohesive fracture energies are similarly graded, using the relationship between G_{co} and the graded moduli E in brittle materials (equation (10)). We further assume that the interfacial fracture energy G_{ad} is constant throughout the laminate, and can be estimated for brittle materials by equation (11).

Substituting the graded expressions for E , \bar{E}_1 , and \bar{E}_2 in equations (3) and (12), we get the cohesive and adhesive failure stresses for a structure with linearly graded moduli and corresponding graded cohesive fracture energies:

$$\begin{aligned}\sigma_{co} &= \left[\frac{\bar{G}_{co} \bar{E}}{\pi c} \frac{1 + (2c/d - 1) \Delta E / \bar{E}}{1 + (c/d - 1) \Delta E / \bar{E}} \right]^{1/2} \\ \sigma_{ad} &= \left[\frac{4G_{ad} \bar{E}}{c} \left(1 - \frac{c}{d}\right) \frac{1 + (c/d) \Delta E / \bar{E}}{1 + (c/d - 1) \Delta E / \bar{E}} \right]^{1/2}\end{aligned}\quad (33)$$

depicted in figure 3. Plane stress condition was assumed for the cohesive failure, and the crack initiation factor $\sqrt{2}$ was inserted in the adhesive failure stress. The ratio $\Delta E / \bar{E}$ may assume values from -1 to 1 .

Similarly, the deflection condition for a structure with linearly graded moduli and corresponding graded cohesive fracture energies is given by substituting the expressions for E and \bar{E}_2 in equation (14):

$$\frac{G_{ad}}{\bar{G}_{co}} < \frac{1}{4\pi(1-c/d)} \frac{1 + (2c/d - 1) \Delta E / \bar{E}}{1 + (c/d) \Delta E / \bar{E}} \quad (34)$$

depicted in figure 4. This deflection condition can be expressed in terms of the structural resilience R defined in equation (17):

$$\frac{G_{ad}}{\bar{G}_{co}} = \frac{1}{4\pi R} \frac{1 + (1 - 2R) \Delta E / \bar{E}}{1 + (1 - R) \Delta E / \bar{E}} \quad (35)$$

leading to $R = R(G_{ad}/\bar{G}_{co}, \Delta E/\bar{E})$, mapped in figure 4 (the details of this expression are not shown as they are not instructive).

Fiber volume fraction in a Bouligand

The tilting rotation of laminae induces an angular gap between adjacent laminae, which effectively reduces the fiber volume fraction in a Bouligand. The mean effect of tilting on the volume fraction can be estimated in the following way. Considering a total laminae twisting range of 180° , the total height of a Bouligand is $t \cong mD + 2w$, where m is the number of laminae in the Bouligand, w is the lamina width, and D is its thickness (equal to the fiber diameter) (figures 6(c) and (d)). The angular gap between adjacent laminae is $\delta_\varphi \cong \pi/m$, enclosing a triangular

cross sectional area of $a \cong w^2 \delta_\varphi / 2 \cong \pi w^2 / 2m$. The rectangular cross sectional area of the lamina is $b = wD$, so that the lamina volume fraction in a Bouligand is $b/(b+a)$. Finally, the fiber volume fraction in a lamina is $\pi/4 \cong 0.78$ (assuming square packing), and hence the fiber volume fraction in a Bouligand is given by:

$$V_f \cong \frac{\pi}{4} \frac{1}{1+a/b} \cong \frac{\pi}{4} \left[1 + \frac{\pi/2}{t/w - 2} \right]^{-1}. \quad (36)$$

ORCID iDs

Israel Greenfeld  <https://orcid.org/0000-0001-9683-7267>

H Daniel Wagner  <https://orcid.org/0000-0002-0741-2169>

References

- [1] Wagner H D 2021 Hierarchical interfaces as fracture propagation traps in natural layered composites *Materials* **14** 6855
- [2] Launey M E and Ritchie R O 2009 On the fracture toughness of advanced materials *Adv. Mater.* **21** 2103–10
- [3] Liu Z, Zhang Z and Ritchie R O 2020 Structural orientation and anisotropy in biological materials: functional designs and mechanics *Adv. Funct. Mater.* **30** 1908121
- [4] Evans A G 1990 Perspective on the development of high-toughness ceramics *J. Am. Ceram. Soc.* **73** 187–205
- [5] Clegg W J, Kendall K, Alford N M, Button T W and Birchall J D 1990 A simple way to make tough ceramics *Nature* **347** 455–7
- [6] Mayer G 2006 New classes of tough composite materials—lessons from natural rigid biological systems *Mater. Sci. Eng. C* **26** 1261–8
- [7] Dunlop J W C, Weinkamer R and Fratzl P 2011 Artful interfaces within biological materials *Mater. Today* **14** 70–78
- [8] Barthelat F, Yin Z and Buehler M N R M 2016 Structure and mechanics of interfaces in biological materials *Nat. Rev. Mater.* **1** 16007
- [9] Ritchie R O, Buehler M J and Hansma P 2009 Plasticity and toughness in bone *Phys. Today* **62** 41–47
- [10] Aizenberg J, Weaver J C, Thanawala M S, Sundar V C, Morse D E and Fratzl P 2005 Skeleton of *Euplectella* sp.: structural hierarchy from the nanoscale to the macroscale *Science* **309** 275–8
- [11] Miserez A, Weaver J C, Thurner P J, Aizenberg J, Dauphin Y, Fratzl P, Morse D E and Zok F W 2008 Effects of laminate architecture on fracture resistance of sponge biosilica: lessons from nature *Adv. Funct. Mater.* **18** 1241–8
- [12] Monn M A, Weaver J C, Zhang T, Aizenberg J and Kesari H 2015 New functional insights into the internal architecture of the laminated anchor spicules of *Euplectella aspergillum* *Proc. Natl Acad. Sci. USA* **112** 4976–81
- [13] Weaver J C *et al* 2007 Hierarchical assembly of the siliceous skeletal lattice of the hexactinellid sponge *Euplectella aspergillum* *J. Struct. Biol.* **158** 93–106
- [14] Gao H, Ji B, Jager I L, Arzt E and Fratzl P 2003 Materials become insensitive to flaws at nanoscale: lessons from nature *Proc. Natl Acad. Sci.* **100** 5597–600
- [15] Greenfeld I, Kellersztein I and Wagner H D 2020 Nested helicoids in biological microstructures *Nat. Commun.* **11** 1–12
- [16] Kellersztein I, Greenfeld I and Wagner H D 2021 Structural analysis across length scales of the scorpion pincer cuticle *Bioinspir. Biomim.* **16** 026013

- [17] Kellersztein I, Cohen S R, Bar-On B and Wagner H D 2019 The exoskeleton of scorpions' pincers: structure and micro-mechanical properties *Acta Biomater.* **94** 565–73
- [18] Kendall K 1975 Transition between cohesive and interfacial failure in a laminate *Proc. R. Soc. A* **344** 287–302
- [19] Hutchinson J W, Mear M E and Rice J R 1987 Crack paralleling an interface between dissimilar materials *Trans. ASME, J. Appl. Mech.* **54** 828–32
- [20] He M Y and Hutchinson J W 1989 Kinking of a crack out of an interface *Trans. ASME, J. Appl. Mech.* **56** 270–8
- [21] Matos P P L, Mcmeeking R M, Charalambides P G and Drory M D 1989 A method for calculating stress intensities in bimaterial fracture *Int. J. Fract.* **40** 235–54
- [22] Thouless M D, Cao H C and Mataga P A 1989 Delamination from surface cracks in composite-materials *J. Mater. Sci.* **24** 1406–12
- [23] Nairn J A and Hu S 1992 The initiation and growth of delaminations induced by matrix microcracks in laminated composites *Int. J. Fract.* **57** 1–24
- [24] Ballarini R, Charalambides P G and Islam S 1995 Near-tip dual-length scale mechanics of mode I-cracking in laminate brittle-matrix composites *Int. J. Fract.* **70** 275–304
- [25] Jha M, Charalambides P G and Ballarini R 1997 Near-tip mode-I elastic fields in bimaterial layered systems *Int. J. Solids Struct.* **34** 1849–71
- [26] Bermejo R and Danzer R 2010 High failure resistance layered ceramics using crack bifurcation and interface delamination as reinforcement mechanisms *Eng. Fract. Mech.* **77** 2126–35
- [27] Hutchinson J W and Suo Z 1992 Mixed-mode cracking in layered materials *Adv. Appl. Mech.* **29** 63–191
- [28] Wagner H D and Marom G 1983 Delamination failure in hybrid composites *38th Annual Conf.* (Reinforced Plastics/Composites Institute, The Society of the Plastics Industry)
- [29] Wagner H D 1983 Elastic properties and fracture of hybrid composite materials *PhD Dissertation* Hebrew University of Jerusalem pp 83–90
- [30] Kendall K 1975 Crack-propagation in lap shear joints *J. Phys. D: Appl. Phys.* **8** 512–22
- [31] AFGROW 2002 *DTD Handbook, Handbook for Damage Tolerant Design* (Dayton, OH: AFGROW)
- [32] Ashby M F 2011 *Materials Selection in Mechanical Design* 4th edn (Oxford: Elsevier)
- [33] Melnick C A, Chen Z and Mecholsky J J 2011 Hardness and toughness of exoskeleton material in the stone crab, *Menippe mercenaria* *J. Mater. Res.* **11** 2903–7
- [34] Mazzotta M G, Putnam A A, North M A and Wilker J J 2020 Weak bonds in a biomimetic adhesive enhance toughness and performance *J. Am. Chem. Soc.* **142** 4762–8
- [35] Daniel I M and Ishai O 2006 *Engineering Mechanics of Composite Materials* (New York: Oxford) p 411
- [36] Roylance D 2001 *Introduction to Fracture Mechanics* (Cambridge, MA: Massachusetts Institute of Technology) pp 1–17
- [37] Ameh E S 2020 Consolidated derivation of fracture mechanics parameters and fatigue theoretical evolution models: basic review *SN Appl. Sci.* **2** 1800
- [38] Fracture Mechanics Website Griffith's energy release rate (available at: www.fracturemechanics.org/griffith.html)